Targeting OCA-B/Pou2af1 blocks type-1 diabetes and reduces infiltration of activated, islet-reactive T cells

Heejoo Kim[1,2], Jelena Perovanovic[1,2], Arvind Shakya[1,2], Zuolian Shen[1,2], Cody German[1,2], Andrea Ibarra[1,2], Jillian L. Jafek[1,2], Brian D. Evavold[1], Danny H.-C. Chou[3], Peter E. Jensen[1], Xiao He[1], and Dean Tantin[1,2,*]

[1]Department of Pathology, University of Utah School of Medicine, Salt Lake City, UT 84112, U.S.A.
[2]Huntsman Cancer Institute, University of Utah School of Medicine, Salt Lake City, UT 84112, U.S.A.
[3]Department of Biochemistry, University of Utah School of Medicine, Salt Lake City, UT 84112, U.S.A.

[*]Corresponding authors: Dean Tantin, Department of Pathology, University of Utah School of Medicine, Salt Lake City, UT 84112. E-mail address: dean.tantin@path.utah.edu

Other authors: Heejoo Kim, heejoo.kim@path.utah.edu;

Running title: OCA-B in T1D

Manuscript metadata:

Characters in title (including spaces): 108
Words in abstract: 243
Character count (including spaces): 78,247
Total main figures: 7
Total main tables: 0

Abstract

Autoimmune therapies aim to inhibit autoreactivity while preserving normal immune function. The transcriptional coregulator OCA-B, also known as Bob.1/OBF-1 (gene symbol *Pou2af1*) is induced in stimulated naïve $CD4^+$ T cells, where docks with transcription factor Oct1 to regulate genes such as *Il2* and *Ifng*. Oct1 and OCA-B only regulate their targets in cases of repeated antigen exposure, a necessary feature of autoimmunity. We hypothesized that T cell-specific OCA-B deletion would protect mice from autoimmune diabetes, and that pharmacologic OCA-B inhibition would provide similar protection. We developed a new *Ocab* (*Pou2af1*) conditional allele and backcrossed it onto a diabetes-prone NOD/ShiLtJ strain background. T cell-specific OCA-B loss protected mice from spontaneous T1D. Protection was associated with reduced pancreatic T cell and macrophage infiltration and reduced proinflammatory cytokine expression. We profiled prediabetic pancreatic lymph nodes and islets by single-cell RNA sequencing and T cell receptor clonotype analysis. Although lymph nodes showed minimal differences, activated/memory $CD8^+$ cell specificities known to participate in diabetes pathogenesis failed to emerge in the islets of OCA-B deficient mice. In contrast, diabetogenic $CD4^+$ clones were present, but associated with markers of anergy. The protective effect of OCA-B loss was diminished, or even eliminated, using monoclonal models with high affinity to artificial or neoantigens. Rationally-designed membrane-penetrating OCA-B peptide inhibitors normalized glucose levels, and reduced T cell infiltration and proinflammatory cytokine expression in newly-diabetic NOD mice. Together, the results indicate that OCA-B is a potent autoimmune regulator and a promising target for pharmacologic inhibition.

50 **Introduction**

51 Type 1 Diabetes (T1D) is an autoimmune disease in which the host immune system is directed towards
52 antigens associated with pancreatic beta cells [1, 2]. Pathologically, T1D is characterized by insulitis, beta
53 cell destruction and consequent inability to produce insulin. The main treatment for T1D, life-long
54 insulin therapy, treats symptoms but not cause. The development of new T1D treatments is limited by
55 an incomplete understanding of disease mechanisms [3]. Beta cell regeneration is a promising line of
56 therapy, but is likely to result in renewed autoimmune attack unless methods can be developed to
57 specifically block T1D autoimmunity. An ideal method of therapy would be to capture patients early in
58 the disease course and block autoimmunity while keeping normal immune function intact. Such a
59 therapy would spare remaining beta cell function.

60 In $CD4^+$ T cells, the transcription factor Oct1 and its cofactor OCA-B regulate a set of ~150
61 target genes, including *Il2*, *Ifng*, *Csf2* (*Gmcsf*) and *Il17a* [4]. Upon T cell activation, many of these genes
62 are activated by pathways that converge on the transcription factors NF-AT, AP-1 and NF-κB. These
63 factors can be thought of as the primary on/off switches for these genes. Drugs that block NF-AT
64 activation for example effectively shut down their expression. Such drugs have utility in many
65 contexts, but also have drawbacks including global dampening of immune function and side effects
66 due to the expression of these factors in other tissues. By contrast, Oct1 and OCA-B act by insulating
67 silent genes against stable repression and control gene expression in cases of repeated antigen
68 exposure. Moreover, OCA-B expression is largely confined to lymphocytes, and varies in different T
69 cell populations. OCA-B is not expressed in thymocytes and is undetectable in naïve $CD4^+$ T cells, but
70 is induced and stably expressed after sustained antigen stimulation. Deficiency in either protein does
71 not affect $CD4^+$ T cell responses to stimulation in vitro or primary infection in mice [4, 5]. In contrast,
72 restimulation of previously activated Oct1 or OCA-B deficient cells results in gene expression defects
73 of 100-fold or more [4, 6]. CD4 memory T cell formation is also defective in the absence of either
74 protein, with the few memory cells formed being highly defective in their ability to mount antigen
75 recall responses [4]. Oct1 and OCA-B mediate these effects by recruiting the histone lysine demethylase
76 Jmjd1a/Jhdm2a/Kdm3a to target loci, where it locally removes inhibitory H3K9me2 chromatin marks
77 that would otherwise promote repressive chromatin environments [4, 6]. OCA-B also potentiates
78 polarization of activated helper T cells towards the Th17 phenotype, among the most pro-inflammatory
79 helper T cell subsets [7].

80 Persistent antigen exposure is also a common property of autoimmune responses. Among
81 profiled $CD4^+$ T cell subsets, OCA-B levels are elevated in both central memory cells and pancreas-

82 infiltrating, islet-reactive cells (http://www.immgen.org/databrowser/index.html). Both Oct1 and OCA-
83 B are highly conserved to humans, and genome-wide association studies identify Oct1/OCA-B binding
84 site polymorphisms that confer predisposition to a variety of human autoimmune diseases including
85 type-1 diabetes (T1D), multiple sclerosis, lupus, inflammatory bowel disease and rheumatoid arthritis
86 [8, 9, 10, 11, 12, 13, 14]. Other studies implicate polymorphisms in or near the *Ocab* (*Pou2af1*) locus itself in
87 different forms autoimmunity [15, 16]. We therefore hypothesized that targeting OCA-B would inhibit
88 over-active, diabetogenic T cell responses.

89 Here, we generated a T cell conditional mouse model of OCA-B deficiency. We show that
90 OCA-B ablation protects animals from spontaneous, polyclonal T1D. Protection was associated with
91 reduced T cell infiltration and proinflammatory cytokine expression. In prediabetic pancreatic lymph
92 nodes, conditional OCA-B deletion maintained normal cell populations, numbers, gene expression and
93 TCR clonality, however deletion in the prediabetic pancreas was associated with significant reductions
94 in the representation of diabetogenic TCR clones such as *Trbv13-3* from the activated/memory $CD8^+$ T
95 cell pool. Non-diabetogenic clones by contrast were increased. In contrast, prodiabetogenic $CD4^+$
96 clonotypes such as *Trbv15*+*Trav13* were associated with anergy in conditional knockouts. Protection
97 from OCA-B loss varied among different TCR transgenic and monoclonal antigen models, and was
98 weakest using synthetic antigens such as ovalbumen, and in monoclonal $CD4^+$ transplant models such
99 as BDC2.5. Protection was stronger, but still incomplete, using a spontaneous CD8-restricted NY8.3
100 TCR transgenic model. Using a rational-design approach, we developed membrane-penetrating OCA-
101 B peptide inhibitors that are efficacious in vitro and in mice. Cumulatively, the results indicate that
102 OCA-B is a potent and pharmacologically accessible autoimmune regulator.

Material and Methods

Laboratory mice

NOD/ShiLtJ, NOD.Scid (NOD.Emv302/2.CB17-Prkdcscid), BDC-2.5 TCR transgenic, NY8.3 TCR transgenic and all breeder mice were maintained in a specific pathogen-free research colony. NCG (NOD-Prkdc^{em26Cd52}Il2rg^{em26Cd22}/NjuCrl) mice were purchased from Charles River Laboratories. NOD.CD4-Cre breeding pairs were a gift from Alexander Chervonsky (University of Chicago). All animal experiments were approved by the University of Utah Institutional Animal Care and Use Committee (IACUC approval 17-05008).

Generation of *Ocab* (*Pou2af1*) conditional mice

Pou2af1$^{tm1a(KOMP)Wtsi}$ mice were provided by the knockout mouse project (KOMP) repository (University of California, Davis). Mice were derived from embryonic stem cell clone EPD0761_3_B03, generated by the Wellcome Trust Sanger Institute. These cells were derived from C57BL/6N mice, but subsequent mouse crosses were to C57BL/6J (>20 generations) for the RIP-mOVA model and NOD (four congenic backcrosses plus an additional backcross to NOD.CD4-Cre). The embryonic stem cells contain a CSD-targeted allele [17]. The presence of WT (582 bp) and Post-FLP (700 bp) alleles was determined by PCR using CSD-Pou2af1-F and CSD-Pou2af1-ttR primers. The presence of the null (801 bp) allele was determined using CSD-Pou2af1-F and CSD-Pou2af1-R primers. The presence of the floxed (359 bp) allele was determined using CSD-Lox-F and CSD-Pou2af1-R primers. Primer sequences were as follows: CSD-Pou2af1-F, 5'TACAGAGAGACTAGACACGGTCTGC; CSD-Pou2af1-R, 5'GATGAGGACTCTGGGTTCAGAGAGG; CSD-loxF, 5'GAGATGGCGCAACGCAATTAATG; CSD-Pou2af1-ttR, 5'AGAAGGCCTCGTTACACTCCTATGC. *Ocab* conditional mice were bred with mice expressing Cre under the control of the CD4 promoter.

Backcrossing *Ocab* germline null and conditional mice to the NOD background

To generate *Ocab*$^{-/-}$ and *Ocab* conditional mice on the NOD background, the previously described C57BL/6 *Ocab* germline null allele [18] and the newly-generated *Ocab* conditional allele were backcrossed to NOD ShiLt/J mice using congenic markers based on Mouse Genome Informatics (http://www.informatics.jax.org) (**Supplemental Table 1**).

Diabetes development and assessment

136 Diabetes was monitored using blood glucose test strips (Contour, Bayer). Mice with blood glucose
137 levels >250 mg/dL were considered diabetic.
138
139 **Leukocyte isolation and intracellular cytokine staining**
140 Pancreatic lymph nodes were grinded and passed through a nylon strainer. Pancreatic leukocytes were
141 isolated as described previously [19]. Briefly, pancreata were chopped and digested using collagenase IV
142 (1 mg/mL, Gibco) in DMEM containing 1% fetal bovine serum (FBS, Rocky Mountain Biologicals)
143 and 10 units of DNase I for 15 min at 37°C. The digested tissues were passed through a 70 μm strainer.
144 Red blood cells were lysed by ACK (Ammonium-Chloride-Potassium) lysis buffer (150 mM NH_4Cl,
145 10 mM $KHCO_3$, 0.1 mM Na_2EDTA). For intracellular cytokine staining, cell suspensions in RPMI
146 medium supplemented with 10% FBS were re-stimulated for 4 hr with phorbol 12-myristate 13-acetate
147 (PMA, Sigma, 50 ng/mL) and ionomycin (Sigma, 1 μg/mL) in the presence of Brefeldin-A (GolgiPlug,
148 BD Bioscience, 1 μl/ml), and fixed by cell fixation/permeabilization solution (BD Cytofix/Cytoperm)
149 according to the manufacturer's protocol. Antibodies used for flow cytometry were as follows: FITC-
150 conjugated anti-mouse CD4, PE-conjugated anti-mouse CD45, PE-conjugated anti-mouse FR4
151 (Biolegend), PerCP-conjugated anti-mouse CD8a, APC-conjugated anti-mouse IFNγ, PE-conjugated
152 anti-mouse IL-17, PerCP-conjugated anti-mouse CD11b, APC-conjugated anti-mouse F4/80, PE-
153 conjugated anti-mouse Gr-1, PE-conjugated anti-mouse ICOS (eBioscience), PerCP-conjugated anti-
154 mouse FoxP3, V450-conjugated anti-mouse CD73 (BD Bioscience).
155
156 **T cell adoptive transfer**
157 6–8 wk old NOD.Scid recipient mice were injected retro-orbitally with 2×10^5 of splenic $CD4^+CD25^-$ T
158 cells from pre-diabetic *Ocab*$^{-/-}$ or *Ocab*$^{+/+}$ NOD.BDC2.5 donors (6–8 wk old, sex-matched). T cells
159 were purified using a $CD4^+CD25^+$ T cell isolation kit (Miltenyi). For $CD4^+CD25^+Foxp3^+$ T cells,
160 1.5×10^6 purified splenic $CD4^+$ T cells from pre-diabeti, BDC2.5 transgenic NOD.*Ocab*$^{-/-}$ or
161 NOD.*Ocab*$^{+/+}$ mice were transferred to sex-matched 6-8 wk old NCG recipients (University of Utah
162 pre-Clinical Resource Core) as previously described [20]. For total splenic transfer experiments, 5×10^6
163 splenocytes from pre-diabetic NOD.*Ocab*$^{fl/fl}$ or NOD.*Ocab*$^{fl/fl}$; CD4-Cre mice were transferred into sex-
164 matched 6-8 week-old NOD.Scid recipients mice as described previously [20].
165
166 **In vivo Treg depletion**

167 Anti-CD25 antibody in PBS (1 mg/mouse, Clone PC61, BioXCell) was administered intraperitoneally
168 to NOD.*Ocab*$^{fl/fl}$ or NOD.*Ocab*$^{fl/fl}$;CD4-Cre mice twice (10 and 17 d after birth) as previously described
169 [21].
170
171 **In vitro culture of CD4 T cells**
172 For anergic cell induction, spleens were harvested from NOD.*Ocab*$^{fl/fl}$;CD4-Cre or control
173 NOD.*Ocab*$^{fl/fl}$ animals. Single-cell suspensions were generated by grinding and passage through 70 µm
174 strainers. CD4$^+$ T cells were isolated using a mouse CD4$^+$ T cell isolation kit (Miltenyi Biotec).
175 Isolated CD4$^+$ T cells were cultured and stimulated with 5 µg/ml plate-bound anti-CD3ε (BD
176 Bioscience) and/or 2 µg/ml anti-CD28 antibodies (eBioscience) as described previously [5]. For OCA-B
177 inhibitor peptide treatments, naïve CD4 T cells were isolated from WT C57BL/6 mice using a mouse
178 naïve CD4$^+$ T cell isolataion kit (Miltenyi Biotec) and cultured as described previously [6]. For the in
179 vitro experiments with OCA-B inhibitor peptides, indicated concentrations of OCA-B inhibitor or
180 control peptides were incubated with cells, with media changes every 2 days after primary stimulation.
181 Activation of C57BL/6 CD4$^+$ cells and subsequent profiling of anergic responses was performed
182 identifically to [5].
183
184 **Single cell RNA sequencing**
185 CD3$^+$ T cells were isolated from 8 week-old NOD.*Ocab*$^{fl/fl}$ or NOD.*Ocab*$^{fl/fl}$; CD4-Cre females using a
186 pan T cell isolation kit (Miltenyi). CD45$^+$ pancreatic leukocytes were isolated from 12 week-old
187 NOD.*Ocab*$^{fl/fl}$ or NOD.*Ocab*$^{fl/fl}$; CD4-Cre females were isolated by flow cytometry using a FACS Aria
188 instrument (Becton-Dickinson). For each condition, cells were isolated from three mice and combined.
189 Cells were processed using the 10× Genomics Chromium platform according the manufacturer's
190 instructions. Paired-end high-throughput sequencing (125 cycles) was performed via an Illumina
191 NovaSeq instrument. Sequencing reads were processed by using 10× Genomics CellRanger pipeline
192 and further analyzed using the Seurat R package. Analysis of cells used a standard filtering protocol
193 removing cells with unique feature counts of >4,000 or <500, as well as cells that have >5%
194 mitochondrial counts (indicative of dead cells). No more than 15% of total cells were removed by this
195 process.
196
197 **OCA-B mutagenesis and co-IP**
198 For generation of the OCA-B double point mutant, a plasmid transiently expressing human OCA-B,
199 pCATCH-Bob.1 [22], was sequentially mutagenized using QuickChange (ThermoFisher). Correct

200 mutagenesis and lack of additional mutations was confirmed by resequencing. Protein expression was
201 confirmed by transiently transfect HCT116 cells, which do not express endogenous OCA-B. HCT116
202 lysate preparation, co-immunoprecipitation of OCA-B and endogenous Jmjd1a, and immunoblot
203 detection was performed using the same conditions as described [4]. For co-IP using M12 cells, lysis
204 buffer consisted of 50 mM Tris-Cl, pH 7.4, 150mM NaCl, 0.5%NP-40, 1 mM EDTA,1 mM EGTA,
205 plus protease/phosphatase inhibitors (PhosSTOP, Roche). Lysates were incubated with 2.5 µg Jmjd1A
206 antibody (Bethyl) and protein-G Dynabeads (ThermoFisher) in lysis buffer containing 20% glycerol
207 overnight at 4°C. After overnight incubation, the indicated concentrations of peptide or PBS vehicle
208 was added and incubated for a further 3 hr at 4°C prior to bead precipitation and washing 3× in lysis
209 buffer plus 20% glycerol. Co-precipitated OCA-B was analyzed by SDS-PAGE and immunoblot.
210
211 **OCA-B inhibitor peptide synthesis**
212 Unique chemically synthesized peptide sequences were as follows: Peptide#1, ARPYQGVRVKEPVK;
213 Peptide#2/JumOCA, VKELLRRKRGH; Peptide#3, ARPYQGVRVKEPVKELLRRKRGH; Scrambled
214 peptide, VLREKGKRHLR. Peptides were synthesized with and without a covalent C-terminal linker
215 and Tat membrane-penetrating peptide (GSG-GRKKRRQRRRGY). Fmoc protected amino acids were
216 obtained from Protein Technologies Inc. 1-[Bis(dimethylamino)methylene]-1H-1,2,3-triazolo[4,5-
217 b]pyridinium 3-oxid hexafluorophosphate (HATU) was purchased from Chemimpex Inc. H-Rink-
218 Amide-ChemMatrix (RAM) was purchased from Biotage. N,N-diisopropylethylamine (DIEA),
219 dichloromethane (DCM), triisopropylsilane (TIS) were purchased from Sigma Aldrich.
220 Dimethylformamide (DMF), trifluoroacetic acid (TFA), acetonitrile (ACN), and ethyl ether were
221 purchased from Fisher Scientific.
222 Peptides were synthesized using automated Fmoc SPPS chemistry on synthesizer (Syro I). Briefly, 220
223 mg of RAM resin (Loading = 0.45 mmol/g) was swelled in DCM for 15 min and followed by adding in
224 a solution of specific Fmoc protected amino acid (AA = 0.1 mmol, DIEA = 0.2 mmol in DCM = 4 mL)
225 and incubated at room temperature for 1.5 h. Then the resin was washed with DMF and DCM and
226 incubated with 5 mL of DCM containing 16% v/v MeOH and 8% v/v DIEA for 5 min. This action was
227 repeated for 5 times before thoroughly washed with DCM and DMF. Then the resin was set to
228 synthesizer for automated synthesis. Coupling reactions were performed using HATU (5 eq.), DIPEA
229 (10 eq.) and amino acid (5 eq.) in DMF with 15 min heating to 70 oC (50 oC for Cys). Deprotection
230 reaction was performed using 20% (v/v) Piperidine in DMF, 5 min rt for 2 rounds. Peptides were
231 cleaved from the resin by treatment with a cocktail buffer (3 mL/0.1 mmol, TFA:H2O:TIS:EDT =
232 95:2:2:1) for 2.5 h. Peptide-TFA solution was then filtered and precipitated in cold ether, and

233 centrifuged and washed with ether twice and vacuum-dried. The crude product was then purified by
234 RP HPLC. Peptides characterization was performed by LC/MS on an Xbridge C18 5 µm (50 x 2.1
235 mm) column at 0.4 mL/min with a water/acetonitrile gradient in 0.1% formic acid on an Agilent 6120
236 Quadrupole LC/MS system. Fractions collected from HPLC runs were also analyzed by LC/MS. The
237 purified fractions containing the targeted product were collected and lyophilized using a Labconco
238 Freeze Dryer. All samples were analyzed by the following conditions: Preparative reverse phase HPLC
239 of crude peptides was performed on a Jupiter 5 µ C18 300 Å (250×10 mm) column at 3 mL/min with a
240 water/acetonitrile (ACN) gradient in 0.1% TFA on an Agilent 1260 HPLC system. Purity, isomer co-
241 injection and stability checks were performed on HPLC on Phenomenex Gemini C18 3 µm (110 Å
242 150×3 mm) column.
243
244 **OCA-B inhibitor peptide treatment**
245 Anesthetized pre-diabetic WT NOD females with glucose levels newly-risen to between 225 to 275
246 mg/dL were treated with the inhibitor or control peptides by intravenous (retro-orbital) injection, 3
247 times every 12 hr. Blood glucose levels were measured at every injection. 4 hr after the last injection,
248 pancreata and pancreatic lymph nodes (PLNs) were collected and cell populations were analyzed by
249 flow cytometry.
250
251 **Statistical analyses**
252 All error bars denote ± SEM. Two-tailed student T-tests were used to ascribe statistical significance.
253 For all figures, *=*p*-value ≤0.05; **=*p*-value ≤0.01.

254 **Results**

255 **Generation of an *Ocab* conditional allele and NOD backcrossing**

256 We generated a conditional *Ocab* (*Pou2af1*) mouse allele using embryonic stem cells provided by the
257 knockout mouse project (KOMP) repository. Deletion of the *LoxP* sites is predicted to create a null
258 allele by disrupting the first three exons (**Supplemental Fig.1A**). Breeding chimeric mice resulted in
259 germline transmission and a founder mouse (Fig.1B, lane 2) that was crossed to a FLP deleter mouse
260 strain (*Rosa26*-FLP) to remove the reporter cassette and create a floxed conditional allele
261 (**Supplemental Fig.1A and B, lane 3**). Intercrossing these mice generated homozygous *fl/fl* mice
262 (**Supplemental Fig.1B, lane 4**). The mice were crossed to germline Cre deleter mice (Rosa26-Cre) to
263 generate null alleles (**Supplemental Fig.1B, lanes 5 and 6**). Homozygous *fl/fl* mice produce normal
264 amounts of both p34 and p35 isoforms, while no protein of either isoform is present in germline-
265 deleted *Δ/Δ* spleens (**Supplemental Fig.1C, lanes 6-8**). These results indicate that the *fl* allele is fully
266 OCA-B sufficient and the Cre-deleted allele is a null. Crossing the *fl* allele onto a CD4-Cre driver,
267 which deletes in both CD4 and CD8 compartments, resulted in efficient deletion in splenic T cells
268 (**Fig.1A**). These findings indicate that this allele represents a robust system in which to study OCA-B
269 function in T cells.

270 As with most genetically engineered mouse lines, the *Ocab* (*Pou2af1*) conditional allele was
271 generated on a C57BL/6 background. To test the prediction that OCA-B expression in T cells promotes
272 T1D emergence, we conducted speed congenic backcrosses to the NOD strain background. This
273 method allows spontaneous diabetes to be produced rapidly by screening and selecting for 13
274 microsatellite and SNP markers associated with NOD autoimmune susceptibility [24]. Following these
275 markers with specific primer pairs (**Supplemental Table S1**), we produced backcrossed animals with
276 all 13 markers in four generations (**Fig.1B**) that recapitulate spontaneous autoimmunity (not shown).
277 For example, *Idd1*, which maps to the MHC region [25], converted to the homozygous NOD allele after 2
278 backcross generations (**Fig.1B**, lane 3), whereas *Idd13*, which maps near beta-2-microglobulin [26]
279 became NOD homozygous after 4 generations (lane 4). Genotyping identified this fourth-generation
280 backcrossed animal as having all 13 microsatellite markers and the *Ocab* conditional allele
281 (**Supplemental Fig.1D**, #122). This founder animal was crossed to NOD.CD4-Cre and the floxed
282 allele homozygosed in order to delete OCA-B in T cells to assess the effects on T1D. Similar NOD
283 backcrosses, conducted using *Ocab* null mice [18], resulted in OCA-B germline-deficient NOD mice
284 (data not shown). As with the original C57BL/6 OCA-B germline knockout [18], all alleles were viable
285 and fertile with no obvious health issues.

286

287 **NOD mice lacking OCA-B are protected from T1D**

288 To study the effect of T cell-specific OCA-B loss on baseline immune function, we performed single-
289 cell RNA sequencing (scRNAseq) and TCR clonotype analysis using $CD3^+$ T cells isolated from PLNs
290 of pre-diabetic 8 week-old female NOD.*Ocab*$^{fl/fl}$;CD4-Cre or NOD.*Ocab*$^{fl/fl}$ littermate controls. For
291 each group cells from three animals were combined for microfluidics and subsequent sequencing. T
292 cells were isolated from PLNs of three animals in each group and combined for analysis. ~6000
293 knockout and ~3000 control cells were identified in this analysis, most of which comprise naïve CD4
294 and CD8 cells (**Supplemental Fig.2A**, pink and orange), and regulatory T cells (Tregs, green). There
295 was also a small population of activated $CD4^+$+$CD8^+$ cells (green), presumably in the process of
296 exiting the lymph nodes. Other than a small decrease in the percentage of activated $CD4^+$+$CD8^+$ cells
297 (4.4 vs 6.1%), few differences in the populations were observed. None of these populations expressed
298 measurable amounts of *Ocab* (*Pou2af1*) mRNA (not shown), however *Pou2af1* is expressed at low
299 levels in T cells making it difficult capture by scRNAseq. In addition, few changes in gene expression
300 were identified, and the great majority of these were not of immunological interest (**Supplemental
301 Fig.2B, Supplemental Table 2**). We also determined TCR repertoires in these T cell populations,
302 identifying few changes as a whole (**Supplemental Fig.2C**) or in specific sub-populations (not
303 shown). These results indicate that OCA-B loss does not have obvious effects on PLN T cell
304 repertoires or status.

305 T1D onset in NOD mice is spontaneous and acute [27]. To test the impact of OCA-B loss in T
306 cells on spontaneous T1D, we compared incidence in in female NOD.*Ocab*$^{fl/fl}$;CD4-Cre mice, and
307 controls lacking the CD4-Cre driver. Glucose was monitored 2-3 times per week. Using a 250 mg/dL
308 blood glucose cutoff, approximately 60% of *Ocab*$^{fl/fl}$ control mice manifested spontaneous diabetes by
309 24 weeks of age, while no *Ocab*$^{fl/fl}$;CD4-Cre mice became diabetic (**Fig.1C**). Blood glucose was stable
310 in *Ocab*$^{fl/fl}$;CD4-Cre females but began to spike in control mice beginning at week 16, rising to an
311 average of >300 mg/dL by 24 weeks (**Fig.1D,E**). Similar results were observed using female whole-
312 body knockout NOD.*Ocab*$^{-/-}$ compared to *Ocab*$^{+/+}$ littermate controls. While ~80% of control females
313 developed T1D within 24 weeks after birth, only ~20% of NOD.*Ocab*$^{\Delta/\Delta}$ females did so (**Fig.1F**).
314 Cumulatively, the results show that OCA-B expression in T cells is critical for T1D pathogenesis in
315 NOD mice.

316

317 **NOD.*Ocab* conditional mice have fewer islet macrophages and IFNγ–expressing cytotoxic T cells,**
318 **and more Tregs**
319 We sacrificed *Ocab*$^{fl/fl}$;CD4-Cre female mice and controls at 8 and 24 weeks, and determined the
320 frequencies of immune cells in the pacreata. We observed more T cells in the pancreata of OCA-B
321 deficient mice (not shown). This result is understandable because the control mice have annihilated
322 their pool of beta cells, resulting in lack of antigen. We also studied pancreatic macrophages in these
323 mice. Islet infiltration of F4/80^{+}CD11b^{+} macrophages is critical for NOD T1D pathogenesis both in
324 spontaneous and adoptive transfer T1D models [28, 29]. CCL1 expressed in diabetogenic CD4 T cells is
325 known to recruit CCR8-expressing macrophages [30]. Interestingly, OCA-B deletion in stimulated, rested
326 and re-stimulated CD4^{+} T cells decreases *Ccl1* mRNA expression compared to controls
327 (**Supplemental Table S3**). We therefore hypothesized that OCA-B expression in T cells is important
328 for macrophage islet infiltration. Despite the fact that antigen and greater numbers of T cells were
329 present, we observed 5-fold fewer macrophages in 24 week-old NOD.*Ocab*$^{fl/fl}$;CD4-Cre islets (**Fig.2A**
330 **and B**). In contrast, macrophage numbers were unaffected by T cell-specific OCA-B loss in pre-
331 diabetic (8 week) mice (**Fig.2A**).
332 IFNγ is a direct OCA-B target gene [4] and a strong promoter of T1D. Levels of serum and
333 pancreatic IFNγ gradually rise in young NOD mice, reaching maximum at diabetes onset [31].
334 Diabetogenic CD4^{+} and CD8^{+} T cells both express IFNγ in humans and NOD mice [32, 33, 34]. Therefore,
335 we predicted that OCA-B loss would reduce islet IFNγ expression in CD4^{+} and CD8^{+} T cells. We
336 compared IFNγ-expressing pancreatic CD4^{+} and CD8^{+} T cells in female NOD.*Ocab*$^{fl/fl}$;CD4-Cre and
337 littermate control mice lacking CD4-Cre. In 12 week-old prediabetic mice, CD8^{+} T cell frequencies
338 were significantly decreased (**Fig.2C**), whereas CD4^{+} T cells at the same timepoint were unchanged
339 (data not shown). At the time of diabetes onset (16 weeks), proportionally fewer IFNγ-expressing
340 CD8^{+} T cells were present in *Ocab* conditional-deleted mice compared to controls (**Fig.2D**).
341 CD4^{+}CD25^{HI}FoxP3^{+} Tregs interfere with T1D development in NOD mice [35, 36]. Analysis of
342 previously generated RNAseq datasets shows that naïve *Ocab* null CD4^{+} T cells express 4-fold more
343 *Foxp3* mRNA compared to controls upon in vitro stimulation (**Supplemental Table S3**). To determine
344 whether the protection conferred by T cell conditional OCA-B is associated with changes in Tregs, we
345 analyzed pancreatic Treg frequencies, observing a trend towards more Tregs in pre-diabetic (8 week-
346 old) NOD.*Ocab*$^{fl/fl}$;CD4-Cre mice compared to controls (**Fig.2E**). Interestingly, there were no
347 differences late in disease course, at 16 or 24 weeks (data not shown).

348 If increased Treg numbers help mediate protection in NOD.*Ocab*$^{fl/fl}$;CD4-Cre mice, then
349 depletion of these Tregs would be expected normalize T1D pathogenesis in knockout mice relative to
350 controls. Anti-CD25 antibody injection in neonatal mice preferentially depletes Tregs and accelerates
351 T1D onset in NOD mice [21]. Surprisingly, we observed that anti-CD25 antibody-injected
352 NOD.*Ocab*$^{fl/fl}$;CD4-Cre mice were still protected from T1D development relative to controls, though to
353 a lesser degree than in undepleted mice (**Fig.2F**). These results support a conclusion that Tregs partly
354 contribute to the T1D protection in mice lacking OCA-B in their T cells.
355
356 **T cell-specific OCA-B deletion alters the islet-infiltrating TCR repertoire**
357 We performed scRNAseq and TCR clonotype analysis similar to **Supplemental Fig.2**, but using older
358 (12 week) but still pre-diabetic NOD.*Ocab*$^{fl/fl}$;CD4-Cre or NOD.*Ocab*$^{fl/fl}$ littermate control female
359 mice, and using total CD45$^+$ cells isolated from pancreatic islets rather than PLNs. Cells were isolated
360 from four animals per group and combined for microfluidics and sequencing. After filtering, ~6200
361 knockout and ~3800 control cells were identified. Overlaying cell from both genotypes, we used their
362 gene expression profiles to definitively identify multiple cell lineages, including naïve CD4$^+$ + CD8$^+$ T
363 cells, memory/effector CD4$^+$ T cells, memory/effector CD8$^+$ T cells, B cells, macrophages and
364 neutrophils (**Fig.3A**). The biggest relative change in populations was neutrophils, which decreased
365 from 3.4 to 1.4% in conditional knockout iselts (**Fig.3A**). B cells were also decreased, albeit more
366 slightly. These changes were accompanied by an increase in the percentages of CD4$^+$ and CD8$^+$ T cells
367 with naïve phenotypes in conditional knockouts (31.7 vs. 25%). Like endpoint diabetic animals
368 (**Fig.2A-B**), macrophage numbers were decreased but only slightly. Unlike PLNs, prediabetic islets
369 showed significant changes in gene expression between the two groups (**Fig.3B**), the strongest of
370 which occurred in neutrophils (e.g., *Cxcl2*, down), memory/effector CD8$^+$ T cells (*Ccl4*, *Tcrg-v1*, *Itga*,
371 down; *Tcrbv1*, *Trav8n-2*, up), NK T cells (*Klra2*, *Lars2*, down) and γδT cells (*Gzma*, *Gzmb*, *Ccl5*,
372 down).
373 We also profiled TCR clonality in pancreatic T cells. Across total T cells, few changes were
374 observed (**Supplemental Fig.3**), however this was largely to do similar representation in the naïve T
375 cell pool. Isolating just CD4$^+$ and CD8$^+$ effector/memory subpopulations revealed sharp differences.
376 For example, in polyclonal NOD mice CD8$^+$ T cells expressing TBRV13.3 (Vβ8.1) display reactivity
377 to insulin gene related peptide (IGRP), infiltrate iselts and are diabetogenic [37]. This clone was over-
378 represented in the group of antigen-experienced effector + memory CD8$^+$ cells (**Fig.3C**, 20.9% vs
379 8.6%). Based on this information, we repeated the clonotype analysis, but only using the effector +

380 memory $CD8^+$ T cell cluster. We found that the dominant TCR clonotypes used by conditional and
381 control T cells were strikingly different (**Fig.3D**). Clonotype 1 for example corresponds to a TCRα
382 V8N-2 chain paired with TCRβ V1 or V15 and is not thought to be pathogenic. This clonotype was
383 absent in control islets but represented >4% of islet $CD8^+$ effector + memory T cells (**Fig.3D**). The
384 presence of cells with clonotype 1 in the $CD8^+$ cluster overlaid with both genotypes is shown in
385 **Fig.3E**. Clonotype 2 by contrast is associated with the pro-diabetogenic Vβ13.3 β chain. This
386 clonotype was strongly represented in controls (>3%) but absent from the activated/memory $CD8^+$
387 pool of experimental mice (**Fig.3D**). Clonotype 4 is associated with pro-diabetogenic, BDC-reactive
388 $CD4^+$ T cells [38]. In contrast to the effect of OCA-B loss on diabetogenic CD8 clonotypes, this
389 clonotype was enriched in the activated/memory $CD4^+$ pool in experimental mice, but only in the
390 anergic CTLA4- and FR4-expressing sub-population (**Fig.3E**). Cumulatively, these results indicate
391 that OCA-B loss from T cells signicantly skews the landscape of islet effector/memory-like T cells, in
392 particular $CD8^+$ T cells, to an anti-diabetogenic phenotype.
393
394 **Protection conferred by OCA-B loss is model-specific**
395 T1D in NOD mice originates from defective negative selection in developing T cells, resulting in T
396 cell autoreactivity. OCA-B is not expressed in thymocytes and OCA-B loss does not appear to affect T
397 cell development [4]. Therefore, the protective effect of OCA-B loss in T cells likely arises from
398 blunting pre-existing autoreactivity in the periphery. To test the hypothesis that OCA-B loss confers
399 protection in simplified systems, we crossed OCA-B deficient mouse models employing TCR
400 transgenes and model antigens.
401 Depleting Tregs and transferring remaining T cells from BDC2.5 TCR transgenic mice into
402 NOD.Scid mice results in disease after approximately 10 d [20, 39]. We crossed the germline null *Ocab*
403 allele to BDC2.5 mice to test the effect of OCA-B in this model. We transferred $CD4^+CD25^-$ T cells
404 from germline $Ocab^{-/-}$ or $Ocab^{+/+}$ BDC2.5 mice into NOD.Scid recipients, monitoring diabetes
405 emergence. Transplants from both $Ocab^{-/-}$ and control NOD.BDC2.5 mice resulted in equivalent
406 disease kinetics (**Fig.4A**) and severity (not shown). Transferring $CD4^+CD62L^+V\beta^+$ T cells from $Ocab^{-}$
407 $^{/-}$ and control NOD.BDC2.5 mice into NOD.Scid recipients also showed no difference between the
408 experimental and control groups (**Supplemental Fig.4A**). Negative results were also generated by
409 transplanting total $CD4^+$ T cells into immunodeficient NCG recipients (**Fig.4B**). We also tested the
410 effect of T cell conditional OCA-B deletion in a different strain background, C57BL/6J, using the
411 artificial membranous ovalbumin antigen expressed from the rat insulin promoter (RIP-mOVA) [40]. In

412 this experiment, wild-type OVA-reactive CD8$^+$ OT-I T cells were transferred into either *Ocab*$^{fl/fl}$;CD4-
413 Cre or control *Ocab*$^{fl/fl}$ RIP-mOVA mice. Host CD4$^+$ T cells help transferred OT-I T cells promote
414 T1D pathogenesis in this model [41]. Mice were then infected with Lm-OVA to induce strong and
415 synchronous beta cell destruction and loss of glucose control (>400 mg/dL). No differences were
416 observed (**Supplemental Fig.4B**). These results indicate that OCA-B does not act analogously to
417 transcription factors that act as a primary on/off switches, such as NF-AT. Knockouts of these factors
418 would result in broad immunosuppression and protection from T1D in all models. Rather, our results
419 suggest that the effects of OCA-B loss may protect from autoimmunity in specifc contexts, including
420 polyclonal contexts. To test this supposition, we also performed transplant experiments using total
421 splenocytes from polyclonal NOD.*Ocab*$^{fl/fl}$;CD4-Cre mice or controls. Using this transplant system,
422 robust T1D protection with T cell-specific OCA-B loss was observed (**Fig.3C**). This protection was
423 associated with fewer IFNγ-expressing cytotoxic T cells were detected in the islets of OCA-B T cell
424 conditional NOD mice (**Fig.4D**).
425 NY8.3 transgenic mice express a CD8-restricted TCR directed towards IGRP$_{206-214}$ and
426 manifest spontaneous T1D [42]. The NY8.3 clonotype was significantly attenuated in the islets of T cell
427 conditional OCA-B deficient mice (**Fig.3C-E**). We also crossed the *Ocab* germline allele NY8.3,
428 passively monitoring *Ocab*$^{-/-}$ or littermate control *Ocab*$^{+/+}$ NY8.3 mice for T1D development.
429 Significant protection was observed (HR=0.4472, p=0.0352), though the degree of protection was less
430 than in polyclonal models (**Fig.4E**). Together with the observed depletion of autoreactive CD8 clones
431 from OCA-B deficient pancreatic islets, this result indicates that OCA-B promotes T1D in peripheral
432 auto-reactive T cells in part directly through through the CD8$^+$ cells. Using immunoblotting with OCA-
433 B antibodies, we confirmed OCA-B expression in primary splenic C57BL/6 CD8$^+$ T cells. OCA-B is
434 undetectable in naïve splenic CD4$^+$ cells but becomes induced with prolonged activation [4]. Unlike
435 CD4$^+$ cells (Fig.4G, top panels), OCA-B$^+$ could be detected in naïve cells (**Fig.4G**, lane 1). Expression
436 was augmented more rapidly in CD8$^+$ cells upon T cell activation using CD3ε/CD28 antibodies (lane
437 2). Similar to CD4$^+$ cells, expression was stably maintained when the stimulus was removed and cells
438 were rested with IL-2 (lane 6).
439
440 **OCA-B deficiency promotes CD4$^+$ T cell anergy in vitro**
441 Our scRNAseq data indicate that CD8-restricted diabetogenic clones are depleted from the islets of
442 OCA-B T cell conditional mice. In sharp contrast, CD4-restricted clones were increased but associated
443 with an anergic phenotype (**Fig.3E**). Anergy is a peripheral tolerance mechanisms in which T cells that

444 encounter TCR signals without co-stimulation become nonfunctional to protect from autoreactivity [43,
445 44, 45]. Normal naïve primary $CD4^+$ T cells can be activated in culture by TCR and costimulatory
446 receptor activation, e.g. with anti-CD3ε/CD28 antibodies. Providing TCR signals (via immobilized
447 anti-CD3ε monoclonal antibodies) to naïve T cells in culture generates anergic responses [46]. Loss of
448 Oct1, the transcription factor with which OCA-B docks, augments anergic responses in this assay [5]. To
449 determine if OCA-B loss similarly promotes anergic responses, we stimulated naïve splenic $CD4^+$ T
450 cells from germline knockout *Ocab*$^{-/-}$ and control *Ocab1*$^{+/+}$ animals for 48 hr ex vivo using plate-bound
451 anti-CD3ε antibodies without co-stimulation, and restimulated the cells with PMA/ionomycin.
452 Following restimulation, $CD4^+$ T cells lacking OCA-B generated 2.5-fold less IL-2 (**Fig.5A** and **B**),
453 indicating that OCA-B provides a barrier against anergic responses.
454 ICOS (Inducible T-cell Costimulator) has an important role in the induction of T cell anergy
455 and is down-regulated by Oct1 loss in T cells [47, 48, 49]. Similarly in $CD4^+$ cells, elevated expression of
456 FR4 and CD73 is associated with anergy and higher in Oct1-deficient compared to control cells [43, 50].
457 To determine whether OCA-B affects in the protein related to T cell anergy, we harvested pre-
458 activated $CD4^+CD44^+$ T cells from the spleens of *Ocab*$^{fl/fl}$;CD4-Cre and littermate control CD4-Cre
459 animals, and re-stimulated them for 24 hr ex vivo using anti-CD3ε antibodies ± co-stimulation using
460 anti-CD28 antibodies. $CD4^+CD44^+FR4^{hi}CD73^{hi}$ anergic cells were ~2 fold more strongly induced in T
461 cells lacking OCA-B (**Fig.5C**). ICOS levels were similarly elevated in the OCA-B deficient condition
462 (**Fig.5D**). Additionally, and consistent with prior data [5], the expression of the activation marker CD25
463 was decreased (**Fig.5E**). These results suggest that OCA-B loss creates a requirement for CD28 co-
464 stimulation in secondary stimulation situations, effectively instituting higher immune checkpoint
465 thresholds in order for cells to become fully re-activated.
466
467 **Generation of an OCA-B peptide inhibitor**
468 The normal T cell developmental and primary immune response phenotypes observed with OCA-B
469 genetic deletion suggested the possibility of a "therapeutic window" in which targeting OCA-B
470 pharmacologically would leave baseline immune function only minimally affected. Drugs that target
471 transcription factors and protein-protein interactions are now entering clinical use [51, 52]. Pre-clinical
472 membrane-penetrating peptides have also been developed that successfully target transcription factors
473 such as BCL6 [53]. Based on the co-crystal structure of the Oct1 DNA-binding domain, the OCA-B N-
474 terminus and consensus binding DNA [54], we applied rational-design principles to generate a

475 membrane-permeable peptide inhibitor of OCA-B's downstream effector functions in order to target
476 OCA-B pharmacologically.
477 In $CD4^+$ T cells, Oct1 interacts with Jmjd1a in a MEK/ERK-dependent manner [4, 6]. Oct1
478 contains two consensus ERK phospho-acceptor serines. The structure of the Oct1 DNA binding
479 domain complexed with consensus octamer binding site DNA [55] reveals that these Oct1 serines are
480 located in a flexible, solvent-exposed loop (the linker domain), which connects the two DNA binding
481 sub-domains (**Fig.6A**, red dashed line). In contrast with Oct1, OCA-B constitutively interacts with
482 Jmjd1a [4]. The OCA-B N-terminus has been solved in complex with Oct1 and consensus octamer DNA
483 [54]. The crystalized region of OCA-B is known to include regions critical for both Oct1 binding and
484 transcription activity [56]. To identify potential Jmjd1a-interacting OCA-B regions, we aligned the full-
485 length Oct1 and OCA-B amino acid sequences to a region of androgen receptor (AR) known to interact
486 with Jmjd1a [57]. Human AR mutations that cause androgen insensitivity have been mapped to a cofactor
487 interaction surface spanning residues 698-721 [58]. Aligning this sequence to full-length Oct1 identified
488 the linker domain as the top hit (**Fig.6B**), implicating the Oct1 linker as a potential Jmjd1a-interacting
489 surface. The alignment shows conservation of 3 out of 4 sites of deleterious AR mutation (asterisks)
490 with Oct1. The mutation site that is not conserved is a consensus ERK target in Oct1, and a phospho-
491 mimetic glutamic acid residuein AR (blue box). These findings suggest that the Oct1 linker domain
492 constitutes a surface which, when phosphorylated by ERK, interacts with Jmjd1a.
493 As with Oct1, alignment with OCA-B identifies a potential Jmjd1a interacting surface
494 (**Fig.6B**). Unlike Oct1, an OCA-B glutamic acid residue (Glu30) aligns with AR, consistent with the
495 finding that OCA-B constitutively interacts with Jmjd1a in the absence of ERK signaling [4].
496 Furthermore, the OCA-B residues aligning to AR lie on one side of a short, solvent-exposed alpha-
497 helix (**Fig.6A**). Glu30 (red), Leu31 (yellow), Arg34 (blue) and His38 (blue) may therefore constitute a
498 Jmjd1a docking surface. These residues are conserved to humans (**Fig.6C**). We mutated OCA-B L31
499 and R34 to alanines in a transient expression plasmid to test the effect on the Jmjd1a interaction, and
500 transfected the double-point mutant or parent plasmid control into HCT116 cells, which do not express
501 endogenous OCA-B. Control co-IP using Jmjd1a antibodies and wild-type OCA-B confirms the
502 published interaction (**Fig.6D**, lane 5), while the mutant OCA-B protein failed to interact (lane 8). The
503 mutant was expressed equivalently to WT in HCT116 cells (lanes 2, 3). These results show the
504 importance of OCA-B residues 30-38 for the interaction with Jmjd1a.
505 To identify potential OCA-B competitive inhibitors, we synthesized three overlapping peptides
506 corresponding to the OCA-B N-terminus (**Fig.6E**, peptides #1, #2 (hereafter called "JumOCA") and
507 #3), as C-terminal fusions to the HIV Tat protein for membrane permeability [59]. Initial preparations

508 were conjugated to FITC to track the peptide. Incubating peptides with total splenic or pancreatic
509 $CD3^+$ T cells in culture with 45 μM Tat-fused peptide for 15 min resulted in significant concentration.
510 Control OVA-fused peptide showed no such effect (**Supplemental Fig.5**). We then treated splenic
511 $CD4^+$ T cells with the Tat-fused peptides (lacking FITC) in ex vivo culture. Prior work has shown that
512 6 hr restimulation of resting but previously activated cells reveals sensitivity to OCA-B loss [4]. Using
513 this assay with 50 μM JumOCA peptide (every other day with media changes during rest and
514 restimulation) inhibited *Il2* mRNA expression relative to β-actin by ~10-fold (**Fig.6F**, compare Tat
515 peptide to JumOCA). Although treated cells showed no obvious changes in viability, morphology or
516 expansion during the course of the assay (not shown), there was a 2-3-fold nonspecific diminution of
517 activity associated with unfused Tat peptide (**Fig.6F**, compare Tat peptide with no peptide). The Tat
518 membrane-penetrating peptide has been associated with toxicities [53, 60, 61]. Similar results were obtained
519 with the larger peptide #3 but not with peptide #1 (not shown). Peptide #1 is missing residues
520 important for the Jmjd1a interaction based on mutagenesis (**Fig.6B**). For all further experiments, we
521 exclusively used the JumOCA peptide.
522 We then synthesized a Tat-conjugated peptide using a scrambled JumOCA sequence. This
523 peptide has the same amino acid composition, mass and pI, but lacks the OCA-B primary amino acid
524 sequence and should not be able to efficiently complete for Jmjd1a. We used the Tat-only, scrambled
525 and JumOCA peptides in assays similar to **Fig.6F**, except using flow cytometry to assay endpoint IL-2
526 production. JumOCA significantly inhibited IL-2 production relative to the scrambled control,
527 however there were significant toxicities associated with both the scrambled and Tat-only peptides
528 relative to vehicle (**Fig.6G**). A example mouse from this experiment is shown in **Fig.6H**.
529 The above results are consistent with the JumOCA peptide operating through a Jmjd1a
530 competitive inhibition mechanism. To test this directly, we used JumOCA (lacking Tat) in a Jmjd1a
531 co-IP assay. We subjected lysates from mouse M12 B cells, which expresses endogenous OCA-B, to
532 immunoprecipitation with Jmjd1a antibodies, resulting in efficient OCA-B co-IP (**Fig.6G**, lane 3).
533 Compared to vehicle control, (lane 3), application incubation of immunoprecipitate with JumOCA at
534 concentrations as low as 1.25 μg/mL completely eliminated the Jmjd1a-OCA-B interaction (lane 4).
535
536 **An OCA-B peptide inhibitor protects NOD mice from newly-arisen diabetes**
537 By the time symptoms arise in NOD mice, 90-95% of beta cells have been destroyed. Remaining beta
538 cells are rendered nonfunctional due to insulitis. Alleviating this inflammation provides a "honeymoon
539 period" during which glucose homeostasis can be restored. We treated 14-18 week-old littermate

540 female NOD mice whose glucose levels were newly-risen above 225 mg/dL but still below 275 mg/dL
541 with three intravenous injections of 10 mg/kg peptide or Tat-only peptide control. Injections were
542 spaced 12 hr apart. 12 hr after the final injection, blood glucose was collected and flow cytometry
543 performed on the pancreas and PLNs. Strikingly, the inhibitor reversed elevated blood glucose
544 (**Fig.7A**). Control peptide at the same concentration had no effect. Islet T cell infiltration and pro-
545 inflammatory IFNγ and IL-17A cytokine production were strongly reduced by JumOCA peptide
546 treatment compared to controls (**Fig.7B** and **C**). In contrast to the pancreas, PLNs showed no change in
547 T cell numbers or percentages (**Fig.7D**) but similar changes in pro-inflammatory cytokine production
548 (not shown). These data provide evidence that targeting OCA-B is a valid strategy to treat emerging
549 T1D, potentially with minimal side effects, and identify a first-generation inhibitor that is efficacious
550 in vivo.

551 **Discussion**

552 Here we show that targeting OCA-B genetically or pharmacologically can block T1D in mouse
553 models. OCA-B is a transcriptional coregulatory protein named for its strong expression in the B cell
554 lineage, where it is dispensable until after B cell activation, where it is essential for the generation of
555 germinal centers [62]. OCA-B is not expressed during thymic development or in naïve CD4 T^+ cells, but
556 is stably induced upon T^+ cell activation. In contrast, OCA-B is expressed in $CD8^+$ T cells, albeit at
557 lower levels compared to activated T cells. In both populations, OCA-B expression is maintained after
558 T cell stimulation has ceased.

559 In $CD4^+$ T cells, OCA-B associates with the POU-domain transcription factor Oct1 at ~150
560 immunomodulatory genes – among them *Il2*, *Ifng*, *Il17a* and *Csf2* (*Gmcsf*). Unlike transcription factors
561 such as NF-AT, AP-1 and NF-kB that act as primary "on" switches via direct gene activation, OCA-B
562 removes inhibitory chromatin modifications to establish permissive chromatin environments that allow
563 for silent but previously activated targets to be robustly expressed later [4, 6]. More specifically, OCA-B
564 interacts with Jmjd1a/Kdm3a, a histone lysine demethylase that removes inhibitory histone H3 lysine 9
565 methyl marks. OCA-B target gene expression is unchanged upon primary stimulation of cultured Oct1-
566 or OCA-B-deficient T cells, but upon secondary stimulation (a model of antigen reencounter) the
567 normally observed increased expression does not occur [4, 6]. In vivo, OCA-B loss leaves T cell
568 development and pathogen response unaffected, but impairs the establishment of new central memory
569 $CD4^+$ T cells. The few cells that are formed respond poorly to antigen re-encounter [4]. Repeated antigen
570 encounters that drive high levels of proinflammatory cytokines are a key feature of autoimmunity. In
571 both mice and humans, memory or memory-like cells can underlie autoimmunity including T1D [63, 64,
572 65].

573 The NOD model of T1D is spontaneous but only partially penetrant, much like the human
574 disease [66]. 60-80% of female NOD mice develop T1D in standard environments [27]. We find that
575 prediabetic OCA-B T cell deficient NOD mice harbor normal T cell numbers and similar TCR
576 specificities in their PLNs, constent with prior observations that OCA-B deficient T cells are
577 immunocompetent [4]. Nevertheless, T cell conditional OCA-B knockouts are fully protected from
578 spontaneous T1D. Protection is associated with reduced islet leukocyte infiltration and reduced
579 proinflammatory cytokine expression. Whole-body NOD *Ocab* knockouts are also protected from
580 T1D, though to a lesser degree. Prior work showed that OCA-B whole-body knockout protects mice in
581 a MOG/EAE model of multiple sclerosis [67]. In contrast, a second study showed that OCA-B whole
582 body knockout exacerbates systemic, antibody-driven autoimmunity in *Sanroque* mice [68]. The
583 protective vs. exacerbating effects in these models may be due to effects on BCR repertoire [69]. T cell-

584 specific knockout of Oct1, a transcription factor with which OCA-B docks, blocks EAE but leaves
585 responses to infection with neurotropic viruses intact [5]. Together these data indicate that in T cells
586 Oct1 and OCA-B promote autoimmunity including T1D, but that their role in B cells may be more
587 complex. OCA-B is typically expressed ~50-fold higher in B cells compared to T cells. A correctly
588 calibrated dose of competitive inhibitor could therefore be used to selectively blunt T cell-mediated
589 autoimmunity.

590 scRNAseq experiments reveal decreased neutrophil infiltration and an increase in the
591 percentage of T cells with a naïve phenotype in prediabetic OCA-B conditional knockout islets. Gene
592 expression changes were also identified that were consistent with antidiabetogenic effects of OCA-B T
593 cell knockout. For example, the remaining islet neutrophils in knockout mice show strong reductions in
594 *Cxcl2* expression compared to littermate controls. Cxcl2 is a potent neutrophil chemoattactant that
595 promotes T1D in vivo [70, 71], and therefore reductions in Cxcl2 may contribute to the reduced neutrophil
596 representation. Strikingly, OCA-B T cell deficient mice also lacked diabetogenic TCR clones in their
597 activated/memory CD8 pool. Diabetogenic CD4 clonotypes were present but associated with anergy.
598 Consistently, OCA-B loss promotes $CD4^+$ T cell anergy in vitro.

599 BDC2.5 and NY8.3 TCR transgenic mice are simplified monoclonal systems that allow easy
600 tracking of uniform T cell responses to antigens in vivo [72]. To test if OCA-B loss confers protection in
601 simplified monoclonal systems, we crossed the germline OCA-B null allele to these models, as well as
602 to RIP-mOVA transgenic mice on the C57BL/6 background. The latter mice express synthetic
603 membranous chicken ovalbumin in their thymi and pancreatic beta cells[73]. We crossed whole-body
604 null mice to the BDC2.5 transgenic line [74], which expresses a CD4-restricted TCR specific for a hybrid
605 insulin-chromogranin A peptide [75]. BDC2.5 autoreactive cells migrate to the islets and cause insulitis
606 beginning at 3-4 weeks. Due in part to Tregs that have escaped allelic exclusion, in many animals
607 insulitis is limited and does not progress to full-blown T1D. However, transferring $CD4^+CD62L^+V\beta^+$
608 or $CD4^+CD25^-$ T cells from BDC2.5 donor mice into NOD.SCID recipients results in rapid (7-10 d)
609 disease onset [39]. Transplants from both control and OCA-B null NOD/BDC2.5 mice resulted in disease
610 with similar kinetics. Identical results were also generated by depleting $CD25^+$ Tregs, or by
611 transplanting total $CD4^+$ T cells into immunodeficient NCG recipient mice. OCA-B loss also had no
612 effect using the RIP-mOVA model on the C57BL/6 background. This model expresses a synthetic
613 antigen, membranous chicken ovalbumin, in thymic epithelial and pancreatic beta cells [40].

614 In contrast to BDC2.5 and RIP-mOVA, NY8.3 transgenic mice carry a monoclonal CD8-
615 restricted TCR directed towards $IGRP_{206-214}$ and manifest spontaneous T1D [42]. Unlike BDC2.5

616 transplant models, OCA-B T cell conditional NY8.3 mice showed significant protection, though unlike
617 polyclonal NOD mice protection was incomplete. Cumulatively, the results are consistent with a model
618 in which OCA-B loss does not simply block T cell functionality, but rather desensitizes autoreactive T
619 cells. Because transgenic TCR models have fixed affinities to antigens that can be present throughout
620 disease or arise at specific points during disease etiology, they result in graded levels of disease. By
621 shifting the autoreactivity of different T cells along a spectrum of disease potentials, OCA-B loss can
622 result in full or partial protection in models with low and intermediate disease thresholds, whereas
623 models with high disease potentials remain autoreactive. Although protection in some of the more
624 severe models is likely to be inseparable from immunodeficiency, our results show that genetic
625 ablation of OCA-B strongly protects NOD animals from spontaneous T1D, and results in graded
626 protection that drops off with severity of the model. These properties make OCA-B a promising target
627 for pharmaceutical inhibition.

628 Recent work indicates that the prevailing idea that transcription regulators and protein-protein
629 interactions are "undruggable" is erroneous [51, 52, 76]. Pre-clinical membrane-penetrating peptides have
630 also been developed that successfully target transcription factors such as BCL6 [53]. We applied rational-
631 design principles to generate a membrane-permeable competitive peptide inhibitor of the interaction
632 between OCA-B and a downstream effector, Jmjd1a/Kdm3a. We tested the effect of this inhibitor,
633 termed JumOCA, on T1D onset and severity. The JumOCA sequence does not coincide with other
634 sequences in the human or mouse proteome and is not predicted to be strongly immunogenic. Peptide
635 administration into NOD mice protected animals from newly-arisen T1D and significantly reduced
636 islet-infiltrating T cell numbers and cytokine production, while having more mild effects on the PLNs.
637 OCA-B levels in B cells are at least 50-fold higher than in T cells (immgen.org, [77], making it likely that
638 the observed effects are due to inhibition in T cells. The preservation of normal PLN functionality both
639 with peptide treatment and OCA-B genetic ablation suggests a potential therapeutic window in which
640 targeting OCA-B may leave baseline immune function unaffected. While these peptides are unlikely to
641 be used in a clinical setting, they offer proof-of-principle for OCA-B as a therapeutic target, and can be
642 used as tools for the further development of therapeutics.

Acknowledgements

We thank A. Chervonsky (U. Chicago) for the gift of NOD.CD4-Cre mice. We thank J. Marvin and the University of Utah Health Sciences Center Flow Cytometry Core facility for assistance with flow cytometry. We thank M. Hanson and the University of Utah Health Sciences DNA/peptide synthesis core. This work was supported by grants to DT from the Praespero Foundation, Juvenille Diabetes Research Foundation (1-INO-2018-647-A-N) and National Institutes of Health (R01-AI100873).

Author's contributions

DT conceived the study and designed experiments, supervised the study, and provided administrative, technical and material support. HK, AS, AI and JLJ acquired and interpreted the data. JP performed high-level analysis of scRNAseq and TCR clonotype data. CG helped generate critical reagents. BDE, DH-CC, XH and PJ provided material and intellectual support. All authors were involved in writing, reviewing and revising the manuscript.

656 **Figure legends**

657

658 **Figure 1. Loss of OCA-B protects NOD mice from T1D.**

659 A) The *Ocab* (*Pou2af1*) conditional allele on a C57BL/6 background (**Supplemental Figure 1**) was
660 crossed to CD4-Cre. Total splenic $CD4^+$ T cells were isolated from an $Ocab^{fl/fl}$;CD4-Cre animal or a
661 $Ocab^{+/fl}$;CD4-Cre littermate control, and stimulated for 2 d in vitro using plate-bound CD3ε and
662 soluble CD28 antibodies. An OCA-B immunoblot of stimulated total T cells is shown. β-actin is
663 shown as a loading control.

664 B) To generate NOD.*Ocab* conditional mice by speed congenic backcross, microsatellite repeat
665 polymorphisms at the *Idd* loci were tested by PCR using the primers in **Supplemental Table 1**.
666 Backcross generations 2 and 4 (B2 and B4) are shown (lanes 3 and 4), together with parent C57BL/6
667 (lane 1) and target NOD (lane 2) genomic DNA as controls. Images are of different PCR products
668 resolved using agarose or polyacrylamide gel electrophoresis. The B4 animal was also labeled as
669 "122" for the purpose of panel B.

670 C) Kaplan-Meier plot of diabetes-free survival in littermate female NOD.$Ocab1^{fl/fl}$;CD4-Cre (n=12)
671 and NOD.$Ocab1^{fl/fl}$ (n=14) mice. Diabetes criterion was ≥250 mg/dL blood glucose. *P*-value=0.0025.
672 Hazard ratio (HR)=0.1112.

673 D) Avearage blood glucose levels from mice shown in panel C is shown.

674 E) Mean glucose levels in panel D at endpoint (24 weeks of age). *P*=0.0402.

675 F) Percent diabetes-free survival in germline knockout NOD.$Ocab^{-/-}$ (n=16) and control NOD.$Ocab^{+/+}$
676 (n=17) mice were plotted based blood glucose cutoff of ≥250 mg/dL. *P*=0.0023. HR=0.1933.

677

678 **Figure 2. NOD.*Ocab* conditional mice have fewer islet IFNγ expressing CD8 T cells and**
679 **macrophages, and more Tregs compared to controls.**

680 A) Pancreatic islet leukocytes were isolated from 8 week- or 24 week-old littermate female
681 NOD.$Ocab1^{fl/fl}$;CD4-Cre (8 week; n=3, 24 week; n=5) or NOD.$Ocab1^{fl/fl}$ (8 week; n=3, 24 week; n=4)
682 mice and analyzed by flow cytometry. Mean $CD45^+CD11b^+F4/80^+$ cell frequencies are depicted.

683 B) Frequencies of $CD45^+CD11b^+F4/80^+$ cells from representative animals in panel A are shown. Plots
684 were gated on $CD45^+$ cells.

685 C) Mean percentages of total pancreatic-infiltrating $CD8^+$ T cell in 12 week-old NOD.$Ocab1^{fl/fl}$;CD4-
686 Cre or control NOD.$Ocab1^{fl/fl}$ mice are plotted. Cells were independently purified from 3 pancreata and
687 gated on $CD45^+$.

688 D) IFNγ expressing CD8$^+$ T cell percentages in 16 week old-NOD.*Ocab1*$^{fl/fl}$;CD4-Cre (n=3) and
689 littermate control islets (n=5) are shown.
690 E) Percentages of FoxP3-expressing CD4$^+$ T cells in pre-diabetic (8 week) NOD.*Ocab* conditional and
691 control female mice are plotted. N=3 for each group. Mean of results is shown.
692 F) NOD.*Ocab*$^{fl/fl}$ or NOD.*Ocab*$^{fl/fl}$;CD4-Cre pups were treated with anti-CD25 antibodies
693 intraperitoneally on day 10 and 17 after birth to depleted Tregs. Mice were monitored for T1D
694 emergence as in Figure 1. *P*=0.0089. HR=0.1483.
695
696 **Figure 3. T cell conditional OCA-B loss reduces the numbers of activated, autoreactive**
697 **pancreatic islet T cells.**
698 A) scRNAseq was performed using total islet CD45$^+$ cells from prediabetic NOD.*Ocab*$^{fl/fl}$; CD4-Cre or
699 control NOD.*Ocab*$^{fl/fl}$ mice (n=3 for each group). Cell populations were plotted using UMAP (Seurat R
700 package) and percentages in each cluster are shown for each genotype. Different populations were
701 identified using Seurat R package function FindMarkers.
702 B) Four populations from panel (A) were analyzed for differential gene expression. Identified genes
703 are shown as a scatter plot. Significantly differentially expressed genes (adjusted *p*-value <0.05) are
704 shown in red.
705 C) UMAP plots similar to (A) are shown, except cells expressing TCR clonotype 13-3 are shown. The
706 non-naïve (activated+memory) CD8$^+$ cell population identified in (A) is shown in red.
707 D) The percent contribution of the top 21 identified TCR clonotypes to total activated+memory CD8$^+$
708 cells is shown. The V genes comprising the top 6 clonotypes are also shown.
709 E) Cells positive for clonotypes 1-5 are shown for two clusters, non-naïve (activated+memory) CD8$^+$ T
710 cells and CTLA4$^+$FR4$^+$ anergic cells (consisting of mostly CD4$^+$ cells). For each cluster, positive cells
711 are shown in dark blue. An overlay of control and OCA-B deficient cell populations is shown, however
712 because each clonotype is only observed in a single genotype (panel D), all cells can be mapped back
713 entirely to OCA-B deficient or control (clonotypes 1 and 4: OCA-B deficient; clonotypes 2, 3 and 5:
714 control).
715
716 **Figure 4. OCA-B loss protects NOD mice from T1D in spontaneous and polyclonal splenocyte**
717 **transfer models but not in models using transfer of monoclonal autoreactive T cells.**

718 A) 2×10^5 purified $CD4^+CD25^-$ splenic T cells from NOD.BDC2.5.*Ocab*$^{-/-}$ or control
719 NOD.BDC2.5.*Ocab*$^{+/+}$donors were injected retro-orbitally into NOD.Scid (n=6 for each group) mice.
720 Diabetes-free survival (≥250 mg/dL) is shown. *P*=0.4803. HR=∞.
721 B) 1.5×10^6 purified splenic total $CD4^+$ T cells from NOD.BDC2.5.*Ocab*$^{-/-}$ or control donors were
722 transferred into NCG mice (n=5 for each group). Mice were monitored for diabetes development.
723 *P*=0.2899. HR=0.5456.
724 C) Total NOD splenocytes (5×10^6) from prediabetic 6- to 8-wk-old sex-matched NOD.*Ocab1*$^{fl/fl}$;CD4-
725 Cre or control NOD.*Ocab1*$^{fl/fl}$ donors were adoptively transferred into sex-matched NOD.Scid (n=7 for
726 each group) recipients. Diabetes incidence rates are shown. *P*=0.0017. HR=0.05427.
727 D) At 13 weeks post-transfer, the proportion of IFNγ-expressing $CD8^+$ T cells was assessed by flow
728 cytometry in pancreata isolated from mice receiving splenocytes from NOD.*Ocab1*$^{fl/fl}$;CD4-Cre or
729 NOD.*Ocab1*$^{fl/fl}$ donors in panel C.
730
731 **Figure 5. OCA-B loss in $CD4^+$ T cells increases anergy in vitro.**
732 A) Naïve OCA-B deficient and control $CD4^+$ T cells were stimulated in vitro with anti-CD3ε
733 antibodies. 48 hr later, the cells were re-stimulated with PMA and ionomycin, and analyzed by flow
734 cytometry. Representative frequencies of cytokine expressing $CD4^+$ $CD44^+$ cells are shown.
735 B) Quantitatition using independently purified cells from the spleens of 4 mice treated similar to (A).
736 C) OCA-B deficient and control $CD4^+$ T cells were stimulated in vitro with indicated antibodies, and
737 analyzed by flow cytometry. Mean of $FR4^{hi}$ $CD73^{hi}$ $CD4^+$ $CD44^+$ cell frequencies are shown using
738 independently purified cells from the spleens of 3 mice, with two technical culture replicates
739 performed for each mouse (n=6).
740 D) Similar to panel (C), except frequencies of $CD4^+CD44^+ICOS^+$ cells are plotted.
741 E) Similar to panel (C), except average percentage of $CD4^+CD44^+CD25^+$ cells are plotted.
742
743 **Figure 6. Design and validation of OCA-B peptide inhibitors.**
744 A) OCA-B N-terminus/Oct1 DNA binding domain/octamer binding DNA co-crystal structure (PDB
745 ID 1CQT) (48). Gray: DNA. Green: Oct1 DNA binding domain. Cyan: OCA-B. Structured OCA-B N-
746 and C-termini (residues 16 and 38) are labeled. Relevant OCA-B residues from panel B are
747 highlighted. Red dashed line shows position of the Oct1 linker domain.
748 B) Top alignment of the human androgen receptor (AR) isoform transcript variant 1 (Sequence ID:
749 ADD26780.1) co-activator interaction domain (residues 698-721) with full-length human Oct1 and

750 OCA-B. The Oct1 linker domain and OCA-B N-terminus most resemble the area of AR that interacts
751 with Jmjd1a. Green serines: putative ERK phospho-acceptor sites. Yellow: similar or identical amino
752 acids. Asterisks: known human point mutations that block coactivator binding and cause androgen
753 insensitivity syndrome in humans. Pairwise alignments were performed using the FASTA algorithm
754 (https://embnet.vital-it.ch/software/LALIGN_form.html) and trimmed for the 3-way overlap.
755 C) Alignment of human and mouse primary OCA-B peptide sequences.
756 D) Co-IP of Jmjd1a with double point-mutant OCA-B and wild-type control. HCT116 cells (which
757 lack endogenous OCA-B) transfected with WT or mutant OCA-B constructs were used. Expression of
758 proteins was checked 48 hrs after transfection by Western blotting. 50 mg protein was loaded in each
759 lane.
760 E) Indicated peptide sequences were synthesized as C-terminal Tat fusions for membrane permeability.
761 Arrows indicate position of mutant in (B) and (D).
762 F) *Il2* mRNA expression in primary $CD4^+$ T cells treated with 50 μM JumOCA peptide was measured
763 relative to β-actin internal standard by RT-qPCR. Cells were stimulated with CD3ε/CD28 antibodies
764 for two days, rested for a further 8 days in the presence of exogenous recombinant IL-2, and
765 restimulated for a further 6 hr. Peptide was included during resting and restimulation only, and
766 replaced every other day with media changes.
767 G) IL-2 cytokine expression in primary $CD4^+$ T cells cultured with 50μM peptide at initial treatment,
768 and with 25μM peptide from the secondary treatment was measured by flow cytometry. Cells were
769 treated similarly to (F) except collection, brefeldin A treatment and processing for flow cytometry
770 occurred 24 hr post-restimulation.
771 H) $CD4^+CD44^+IL2^+$ T cell frequencies from representative samples in panel G are shown. Plots were
772 gated on CD4 and CD44.
773 I) The interaction between OCA-B and Jmjd1a was measured in a co-immunoprecipitation assay. After
774 incubation with protein-G beads, the indicated amounts of peptide or vehicle control were added for a
775 further 3 hr prior to precipitation and washing. 1% input (lane 1) is shown as a control.
776
777 **Figure.7. OCA-B inhibitor peptide injections protect NOD mice from newly-arisen diabetes.**
778 A) 3 doses of 10 mg/kg OCA-B inhibitor peptide (n=4) or control peptide (n=5) were injected retro-
779 orbitally every 12 hr into 12-18 week-old NOD female littermate mice whose glucose levels were
780 newly-risen above 225 mg/dL but still below 275 mg/dL. Glucose levels of peptide injected mice are
781 shown right before each injection, and 12 hr after final injection. Control peptide=Tat alone.

782 B) 4hr after the last injection of peptides in panel A, PLN $CD4^+$ and $CD8^+$ T cell percentagess were
783 analyzed by flow cytometry.
784 C) Mean of islet IL-17 expressing T cells in the same mice as in (B) were analyled by flow cytometry
785 and plotted.
786 D) Similar analysis as (C) for IFNγ.
787

788 **References**

789 1. Lernmark, A. & Larsson, H.E. Immune therapy in type 1 diabetes mellitus. *Nat Rev Endocrinol*
790 **9**, 92-103 (2013).

791 2. Cooke, D.W. & Plotnick, L. Type 1 diabetes mellitus in pediatrics. *Pediatr Rev* **29**, 374-384;
792 quiz 385 (2008).

793 3. Staeva, T.P., Chatenoud, L., Insel, R. & Atkinson, M.A. Recent lessons learned from
794 prevention and recent-onset type 1 diabetes immunotherapy trials. *Diabetes* **62**, 9-17 (2013).

795 4. Shakya, A. *et al.* Oct1 and OCA-B are selectively required for CD4 memory T cell function. *J*
796 *Exp Med* **212**, 2115-2131 (2015).

797 5. Kim, H. *et al.* T cell-selective deletion of Oct1 protects animals from autoimmune
798 neuroinflammation while maintaining neurotropic pathogen response. *J Neuroinflammation* **16**,
799 133 (2019).

800 6. Shakya, A., Kang, J., Chumley, J., Williams, M.A. & Tantin, D. Oct1 is a switchable,
801 bipotential stabilizer of repressed and inducible transcriptional states. *The Journal of biological*
802 *chemistry* **286**, 450-459 (2011).

803 7. Yosef, N. *et al.* Dynamic regulatory network controlling TH17 cell differentiation. *Nature* **496**,
804 461-468 (2013).

805 8. van Heel, D.A. *et al.* Inflammatory bowel disease is associated with a TNF polymorphism that
806 affects an interaction between the OCT1 and NF(-kappa)B transcription factors. *Hum Mol*
807 *Genet* **11**, 1281-1289 (2002).

808 9. Vince, N. *et al.* HLA-C Level Is Regulated by a Polymorphic Oct1 Binding Site in the HLA-C
809 Promoter Region. *Am J Hum Genet* **99**, 1353-1358 (2016).

810 10. Cunninghame Graham, D.S., Wong, A.K., McHugh, N.J., Whittaker, J.C. & Vyse, T.J.
811 Evidence for unique association signals in SLE at the CD28-CTLA4-ICOS locus in a family-
812 based study. *Hum Mol Genet* **15**, 3195-3205 (2006).

813 11. Kiesler, P., Shakya, A., Tantin, D. & Vercelli, D. An allergy-associated polymorphism in a
814 novel regulatory element enhances IL13 expression. *Hum Mol Genet* **18**, 4513-4520 (2009).

815 12. Farh, K.K. *et al.* Genetic and epigenetic fine mapping of causal autoimmune disease variants.
816 *Nature* **518**, 337-343 (2015).

817 13. Maurano, M.T. *et al.* Systematic localization of common disease-associated variation in
818 regulatory DNA. *Science* **337**, 1190-1195 (2012).

819 14. Leon Rodriguez, D.A., Carmona, F.D., Echeverria, L.E., Gonzalez, C.I. & Martin, J. IL18 Gene
820 Variants Influence the Susceptibility to Chagas Disease. *PLoS Negl Trop Dis* **10**, e0004583
821 (2016).

822 15. Games Collaborative, G. *et al.* Linkage disequilibrium screening for multiple sclerosis
823 implicates JAG1 and POU2AF1 as susceptibility genes in Europeans. *J Neuroimmunol* **179**,
824 108-116 (2006).

825 16. Nakamura, M. *et al.* Genome-wide association study identifies TNFSF15 and POU2AF1 as
826 susceptibility loci for primary biliary cirrhosis in the Japanese population. *Am J Hum Genet* **91**,
827 721-728 (2012).

828 17. Testa, G. *et al.* A reliable lacZ expression reporter cassette for multipurpose, knockout-first
829 alleles. *Genesis* **38**, 151-158 (2004).

830 18. Kim, U. *et al.* The B-cell-specific transcription coactivator OCA-B/OBF-1/Bob-1 is essential
831 for normal production of immunoglobulin isotypes. *Nature* **383**, 542-547 (1996).

832 19. Sitrin, J., Ring, A., Garcia, K.C., Benoist, C. & Mathis, D. Regulatory T cells control NK cells
833 in an insulitic lesion by depriving them of IL-2. *J Exp Med* **210**, 1153-1165 (2013).

834 20. Presa, M. *et al.* The Presence and Preferential Activation of Regulatory T Cells Diminish
835 Adoptive Transfer of Autoimmune Diabetes by Polyclonal Nonobese Diabetic (NOD) T Cell
836 Effectors into NSG versus NOD-scid Mice. *J Immunol* **195**, 3011-3019 (2015).

837 21. Mellanby, R.J., Thomas, D., Phillips, J.M. & Cooke, A. Diabetes in non-obese diabetic mice is
838 not associated with quantitative changes in CD4+ CD25+ Foxp3+ regulatory T cells.
839 *Immunology* **121**, 15-28 (2007).

840 22. Gstaiger, M., Knoepfel, L., Georgiev, O., Schaffner, W. & Hovens, C.M. A B-cell coactivator
841 of octamer-binding transcription factors. *Nature* **373**, 360-362 (1995).

842 23. Zhang, C. *et al.* Elimination of insulitis and augmentation of islet beta cell regeneration via
843 induction of chimerism in overtly diabetic NOD mice. *Proc Natl Acad Sci U S A* **104**, 2337-
844 2342 (2007).

845 24. Serreze, D.V. *et al.* B lymphocytes are essential for the initiation of T cell-mediated
846 autoimmune diabetes: analysis of a new "speed congenic" stock of NOD.Ig mu null mice. *J Exp*
847 *Med* **184**, 2049-2053 (1996).

848 25. Hattori, M. *et al.* The NOD mouse: recessive diabetogenic gene in the major histocompatibility
849 complex. *Science* **231**, 733-735 (1986).

850 26. Serreze, D.V. *et al.* Subcongenic analysis of the Idd13 locus in NOD/Lt mice: evidence for
851 several susceptibility genes including a possible diabetogenic role for beta 2-microglobulin. *J*
852 *Immunol* **160**, 1472-1478 (1998).

853 27. Makino, S., Muraoka, Y., Kishimoto, Y. & Hayashi, Y. Genetic analysis for insulitis in NOD
854 mice. *Jikken Dobutsu* **34**, 425-431 (1985).

855 28. Rosmalen, J.G. *et al.* Subsets of macrophages and dendritic cells in nonobese diabetic mouse
856 pancreatic inflammatory infiltrates: correlation with the development of diabetes. *Lab Invest*
857 **80**, 23-30 (2000).

858 29. Peterson, J.D., Berg, R., Piganelli, J.D., Poulin, M. & Haskins, K. Analysis of leukocytes
859 recruited to the pancreas by diabetogenic T cell clones. *Cell Immunol* **189**, 92-98 (1998).

860 30. Cantor, J. & Haskins, K. Recruitment and activation of macrophages by pathogenic CD4 T
861 cells in type 1 diabetes: evidence for involvement of CCR8 and CCL1. *J Immunol* **179**, 5760-
862 5767 (2007).

863 31. Schloot, N.C. *et al.* Serum IFN-gamma and IL-10 levels are associated with disease
864 progression in non-obese diabetic mice. *Diabetes Metab Res Rev* **18**, 64-70 (2002).

865
866 32. Newby, B.N. *et al.* Type 1 Interferons Potentiate Human CD8(+) T-Cell Cytotoxicity Through
867 a STAT4- and Granzyme B-Dependent Pathway. *Diabetes* **66**, 3061-3071 (2017).

868 33. Krishnamurthy, B. *et al.* Autoimmunity to both proinsulin and IGRP is required for diabetes in
869 nonobese diabetic 8.3 TCR transgenic mice. *J Immunol* **180**, 4458-4464 (2008).

870 34. Wang, B. *et al.* Interferon-gamma impacts at multiple points during the progression of
871 autoimmune diabetes. *Proc Natl Acad Sci U S A* **94**, 13844-13849 (1997).

872 35. Brode, S., Raine, T., Zaccone, P. & Cooke, A. Cyclophosphamide-induced type-1 diabetes in
873 the NOD mouse is associated with a reduction of CD4+CD25+Foxp3+ regulatory T cells. *J*
874 *Immunol* **177**, 6603-6612 (2006).

875 36. Jaeckel, E., von Boehmer, H. & Manns, M.P. Antigen-specific FoxP3-transduced T-cells can
876 control established type 1 diabetes. *Diabetes* **54**, 306-310 (2005).

877 37. Wong, C.P., Li, L., Frelinger, J.A. & Tisch, R. Early autoimmune destruction of islet grafts is
878 associated with a restricted repertoire of IGRP-specific CD8+ T cells in diabetic nonobese
879 diabetic mice. *J Immunol* **176**, 1637-1644 (2006).

880 38. Li, L. *et al.* beta cell-specific CD4+ T cell clonotypes in peripheral blood and the pancreatic
881 islets are distinct. *J Immunol* **183**, 7585-7591 (2009).

882 39. Berry, G. & Waldner, H. Accelerated type 1 diabetes induction in mice by adoptive transfer of
883 diabetogenic CD4+ T cells. *J Vis Exp*, e50389 (2013).

884 40. Van Belle, T.L., Taylor, P. & von Herrath, M.G. Mouse Models for Type 1 Diabetes. *Drug*
885 *Discov Today Dis Models* **6**, 41-45 (2009).

886 41. Kurts, C. *et al.* CD4+ T cell help impairs CD8+ T cell deletion induced by cross-presentation of
887 self-antigens and favors autoimmunity. *J Exp Med* **186**, 2057-2062 (1997).

888 42. Verdaguer, J. *et al.* Spontaneous autoimmune diabetes in monoclonal T cell nonobese diabetic
889 mice. *J Exp Med* **186**, 1663-1676 (1997).

890 43. Kalekar, L.A. *et al.* CD4(+) T cell anergy prevents autoimmunity and generates regulatory T
891 cell precursors. *Nat Immunol* **17**, 304-314 (2016).

892 44. Vanasek, T.L., Khoruts, A., Zell, T. & Mueller, D.L. Antagonistic roles for CTLA-4 and the
893 mammalian target of rapamycin in the regulation of clonal anergy: enhanced cell cycle
894 progression promotes recall antigen responsiveness. *J Immunol* **167**, 5636-5644 (2001).

895 45. Kearney, E.R., Pape, K.A., Loh, D.Y. & Jenkins, M.K. Visualization of peptide-specific T cell
896 immunity and peripheral tolerance induction in vivo. *Immunity* **1**, 327-339 (1994).

897 46. Chai, J.G. & Lechler, R.I. Immobilized anti-CD3 mAb induces anergy in murine naive and
898 memory CD4+ T cells in vitro. *Int Immunol* **9**, 935-944 (1997).

899 47. Tuettenberg, A. *et al.* The role of ICOS in directing T cell responses: ICOS-dependent
900 induction of T cell anergy by tolerogenic dendritic cells. *J Immunol* **182**, 3349-3356 (2009).

901 48. Dong, C. & Nurieva, R.I. Regulation of immune and autoimmune responses by ICOS. *J*
902 *Autoimmun* **21**, 255-260 (2003).

903 49. Dong, C. *et al.* ICOS co-stimulatory receptor is essential for T-cell activation and function.
904 *Nature* **409**, 97-101 (2001).

905 50. Martinez, R.J. *et al.* Arthritogenic self-reactive CD4+ T cells acquire an FR4hiCD73hi anergic
906 state in the presence of Foxp3+ regulatory T cells. *J Immunol* **188**, 170-181 (2012).

907 51. Skwarczynska, M. & Ottmann, C. Protein-protein interactions as drug targets. *Future Med*
908 *Chem* **7**, 2195-2219 (2015).

909 52. Green, D.R. A BH3 Mimetic for Killing Cancer Cells. *Cell* **165**, 1560 (2016).

910 53. Polo, J.M. *et al.* Specific peptide interference reveals BCL6 transcriptional and oncogenic
911 mechanisms in B-cell lymphoma cells. *Nat Med* **10**, 1329-1335 (2004).

912 54. Chasman, D., Cepek, K., Sharp, P.A. & Pabo, C.O. Crystal structure of an OCA-B peptide
913 bound to an Oct-1 POU domain/octamer DNA complex: specific recognition of a protein-DNA
914 interface. *Genes Dev* **13**, 2650-2657 (1999).

915 55. Klemm, J.D., Rould, M.A., Aurora, R., Herr, W. & Pabo, C.O. Crystal structure of the Oct-1
916 POU domain bound to an octamer site: DNA recognition with tethered DNA-binding modules.
917 *Cell* **77**, 21-32 (1994).

918 56. Gstaiger, M., Georgiev, O., van Leeuwen, H., van der Vliet, P. & Schaffner, W. The B cell
919 coactivator Bob1 shows DNA sequence-dependent complex formation with Oct-1/Oct-2
920 factors, leading to differential promoter activation. *EMBO J* **15**, 2781-2790 (1996).

921 57. Yamane, K. *et al.* JHDM2A, a JmjC-containing H3K9 demethylase, facilitates transcription
922 activation by androgen receptor. *Cell* **125**, 483-495 (2006).

923 58. Thin, T.H. *et al.* Mutations in the helix 3 region of the androgen receptor abrogate ARA70
924 promotion of 17beta-estradiol-induced androgen receptor transactivation. *The Journal of*
925 *biological chemistry* **277**, 36499-36508 (2002).

926 59. Schwarze, S.R., Hruska, K.A. & Dowdy, S.F. Protein transduction: unrestricted delivery into
927 all cells? *Trends Cell Biol* **10**, 290-295 (2000).

928 60. Caron, N.J., Quenneville, S.P. & Tremblay, J.P. Endosome disruption enhances the functional
929 nuclear delivery of Tat-fusion proteins. *Biochem Biophys Res Commun* **319**, 12-20 (2004).

930 61. Krautwald, S., Ziegler, E., Tiede, K., Pust, R. & Kunzendorf, U. Transduction of the TAT-FLIP
931 fusion protein results in transient resistance to Fas-induced apoptosis in vivo. *The Journal of*
932 *biological chemistry* **279**, 44005-44011 (2004).

933 62. Shi, W. *et al.* Transcriptional profiling of mouse B cell terminal differentiation defines a
934 signature for antibody-secreting plasma cells. *Nat Immunol* **16**, 663-673 (2015).

935 63. Kawakami, N. *et al.* Autoimmune CD4+ T cell memory: lifelong persistence of
936 encephalitogenic T cell clones in healthy immune repertoires. *J Immunol* **175**, 69-81 (2005).

937 64. Yeo, L. *et al.* Autoreactive T effector memory differentiation mirrors beta cell function in type
938 1 diabetes. *J Clin Invest* **128**, 3460-3474 (2018).

939 65. Chee, J. *et al.* Effector-memory T cells develop in islets and report islet pathology in type 1
940 diabetes. *J Immunol* **192**, 572-580 (2014).

941 66. Parker, M.J. *et al.* Immune depletion with cellular mobilization imparts immunoregulation and
942 reverses autoimmune diabetes in nonobese diabetic mice. *Diabetes* **58**, 2277-2284 (2009).

943 67. Ikegami, I., Takaki, H., Kamiya, S., Kamekura, R. & Ichimiya, S. Bob1 enhances
944 RORgammat-mediated IL-17A expression in Th17cells through interaction with RORgammat.
945 *Biochem Biophys Res Commun* **514**, 1167-1171 (2019).

946 68. Chevrier, S., Kratina, T., Emslie, D., Karnowski, A. & Corcoran, L.M. Germinal center-
947 independent, IgM-mediated autoimmunity in sanroque mice lacking Obf1. *Immunol Cell Biol*
948 **92**, 12-19 (2014).

949 69. Casellas, R. *et al.* OcaB is required for normal transcription and V(D)J recombination of a
950 subset of immunoglobulin kappa genes. *Cell* **110**, 575-585 (2002).

951 70. Citro, A. *et al.* CXCR1/2 inhibition blocks and reverses type 1 diabetes in mice. *Diabetes* **64**,
952 1329-1340 (2015).

953 71. Diana, J. & Lehuen, A. Macrophages and beta-cells are responsible for CXCR2-mediated
954 neutrophil infiltration of the pancreas during autoimmune diabetes. *EMBO Mol Med* **6**, 1090-
955 1104 (2014).

956 72. Haskins, K. Pathogenic T-cell clones in autoimmune diabetes: more lessons from the NOD
957 mouse. *Adv Immunol* **87**, 123-162 (2005).

958 73. Kurts, C. *et al.* Constitutive class I-restricted exogenous presentation of self antigens in vivo. *J*
959 *Exp Med* **184**, 923-930 (1996).

960 74. Katz, J.D., Wang, B., Haskins, K., Benoist, C. & Mathis, D. Following a diabetogenic T cell
961 from genesis through pathogenesis. *Cell* **74**, 1089-1100 (1993).

962 75. Delong, T. *et al.* Pathogenic CD4 T cells in type 1 diabetes recognize epitopes formed by
963 peptide fusion. *Science* **351**, 711-714 (2016).

964 76. Zuber, J. *et al.* RNAi screen identifies Brd4 as a therapeutic target in acute myeloid leukaemia.
965 *Nature* **478**, 524-528 (2011).

966 77. Zwilling, S., Dieckmann, A., Pfisterer, P., Angel, P. & Wirth, T. Inducible expression and
967 phosphorylation of coactivator BOB.1/OBF.1 in T cells. *Science* **277**, 221-225 (1997).

968

969

Kim et al. Figure 1

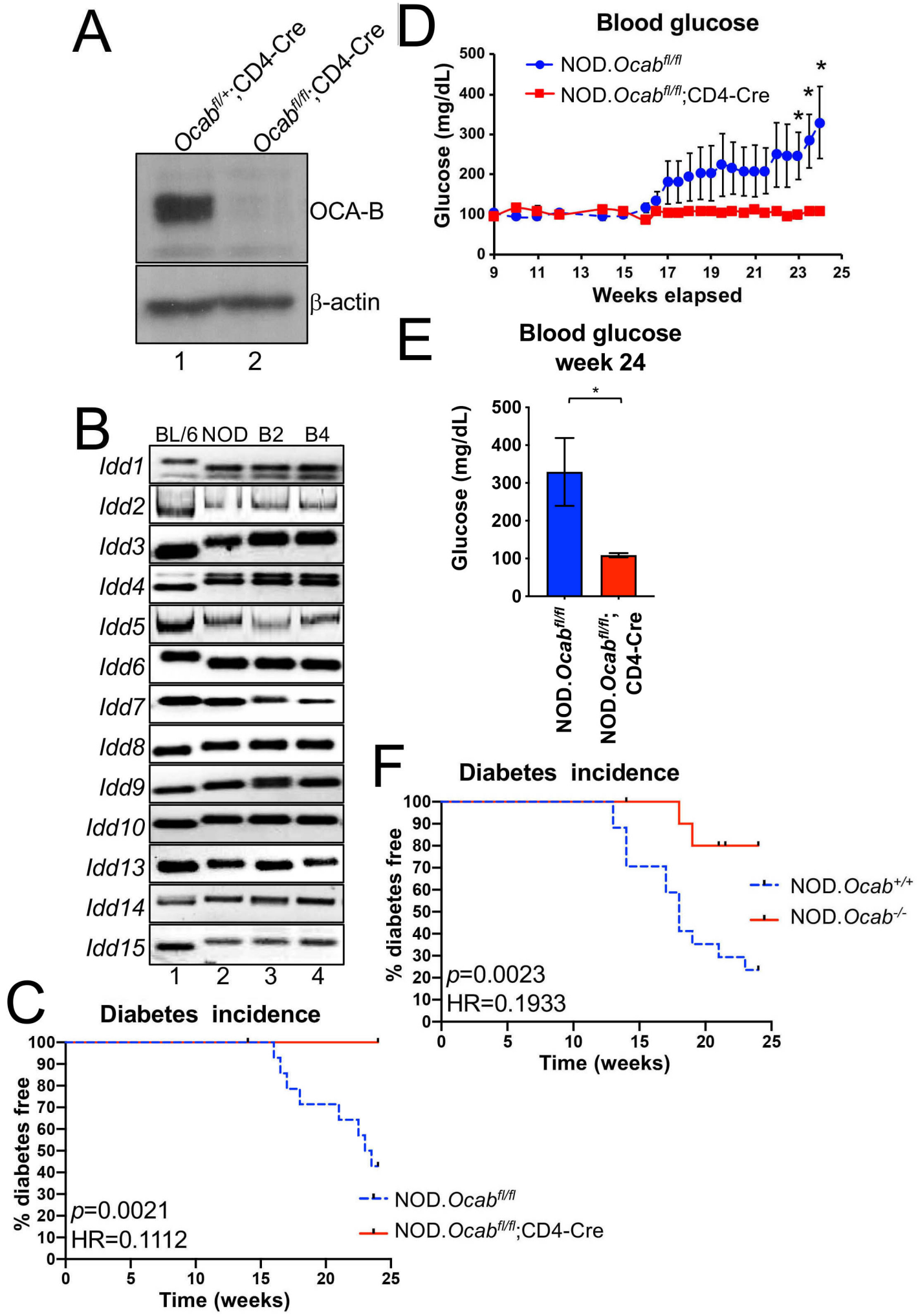

Kim et al. Figure 2

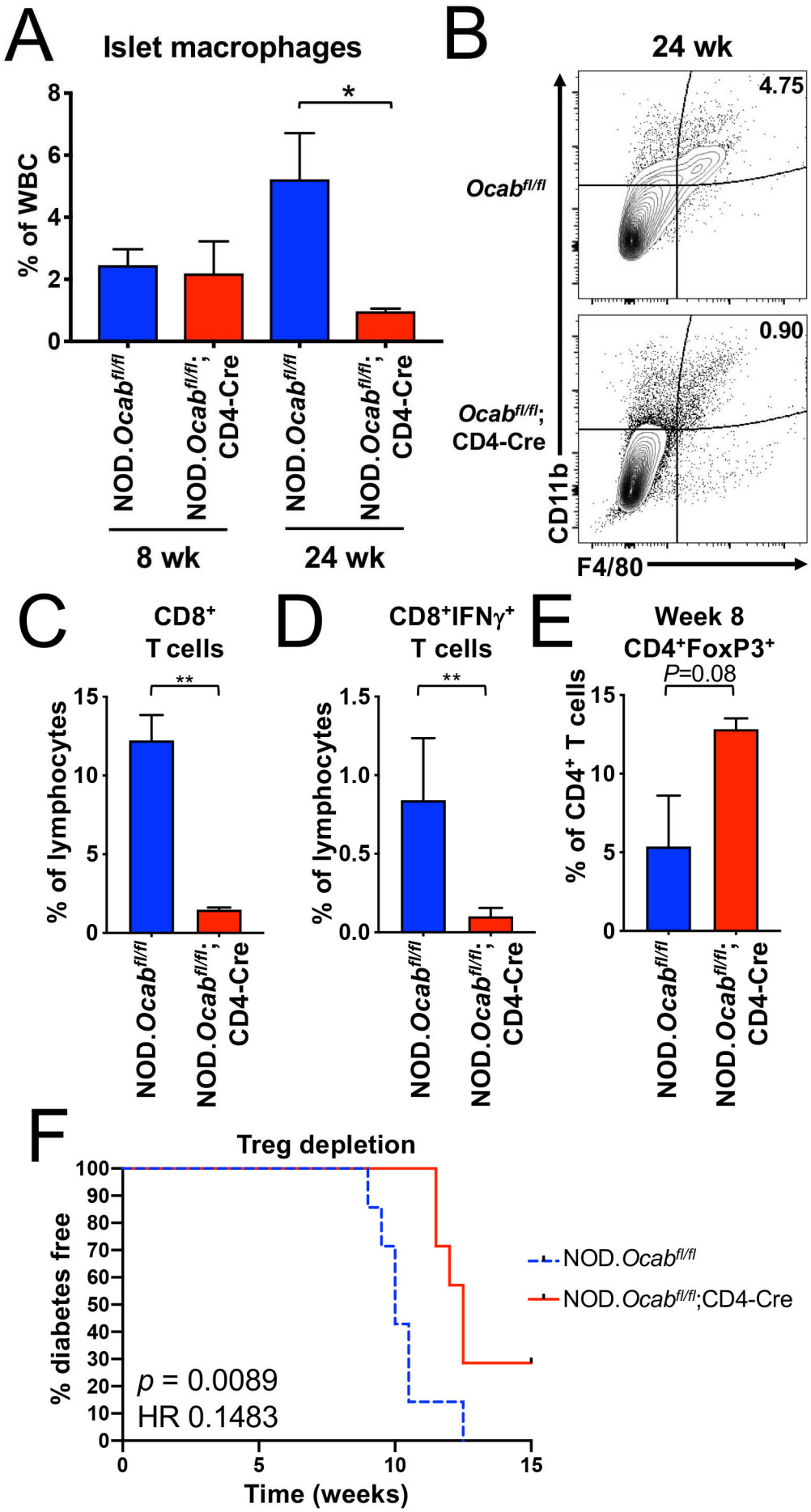

Kim et al. Figure 3

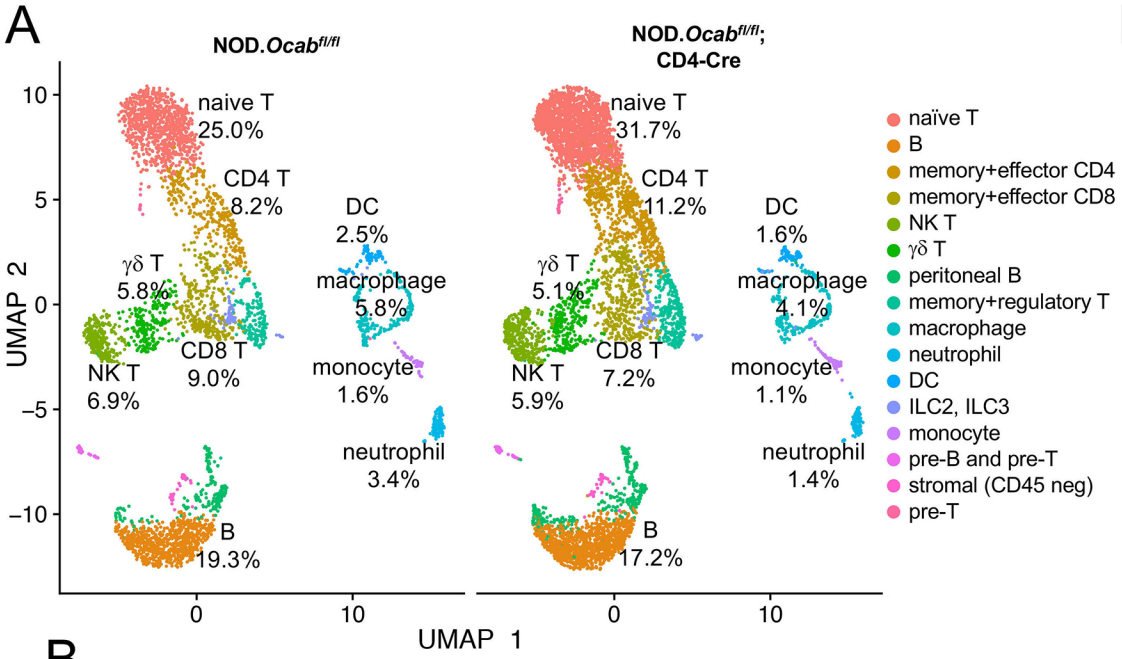

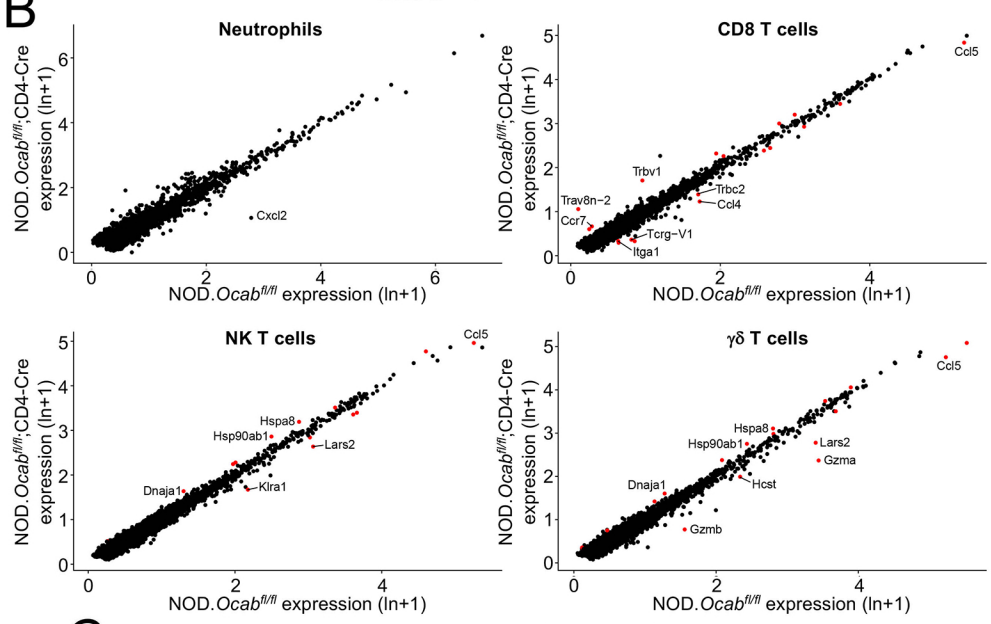

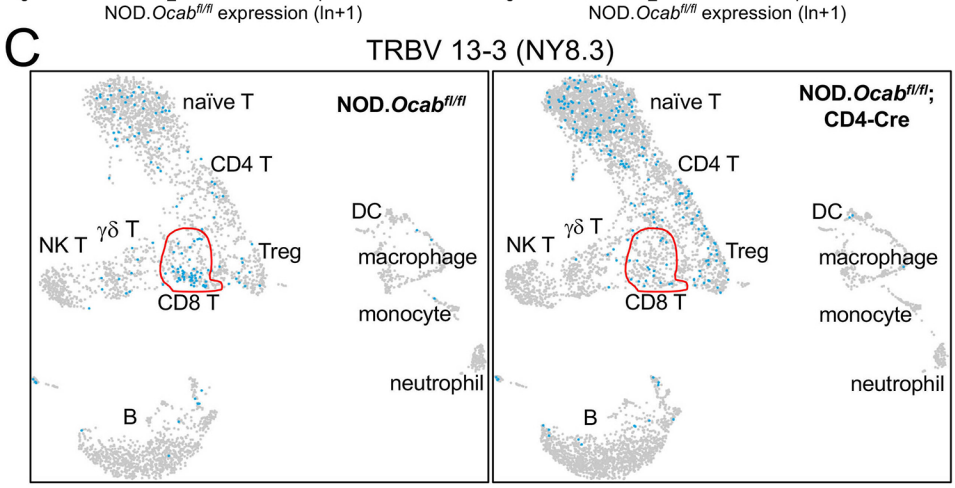

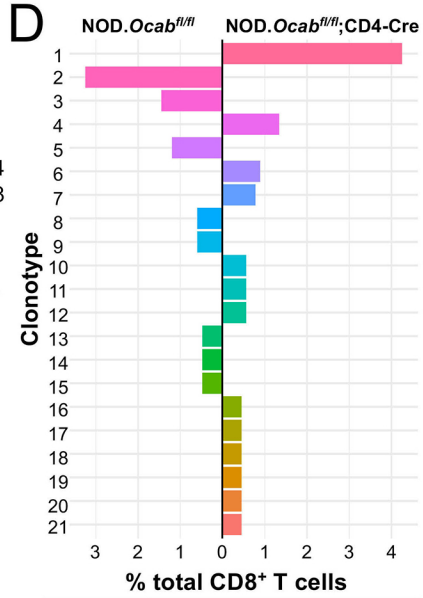

Clonotype	V genes
1	TRAV8N-2;TRBV1;TRBV15
2	TRAV16N;TRBV13-3
3	TRAV9-1;TRBV3
4	TRAV13-1;TRAV16N;TRBV15
5	TRBV13-3

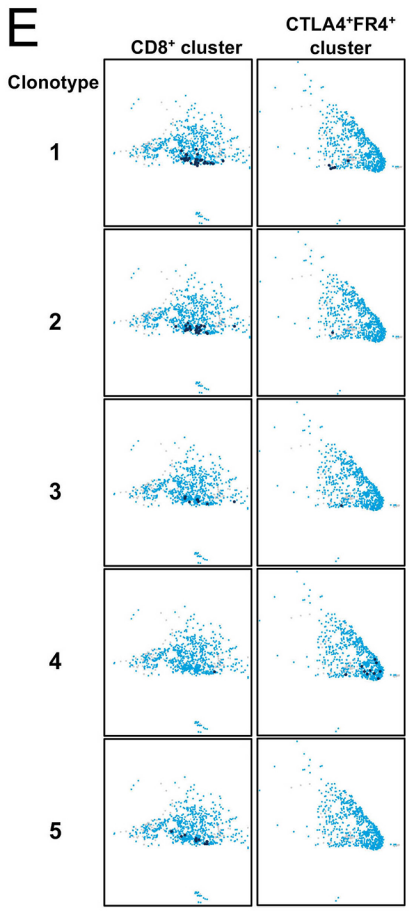

Kim et al. Figure 4

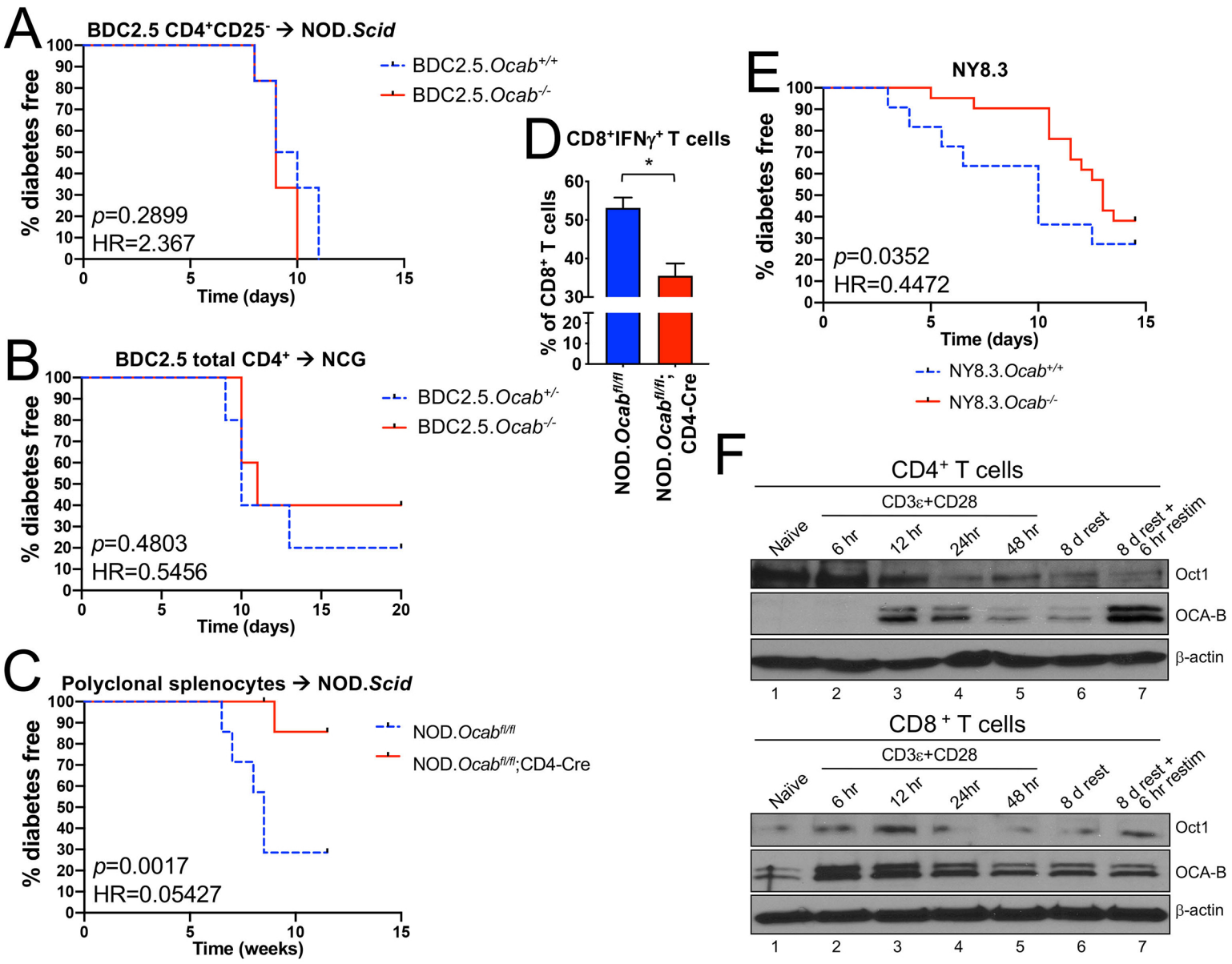

Kim et al. Figure 5

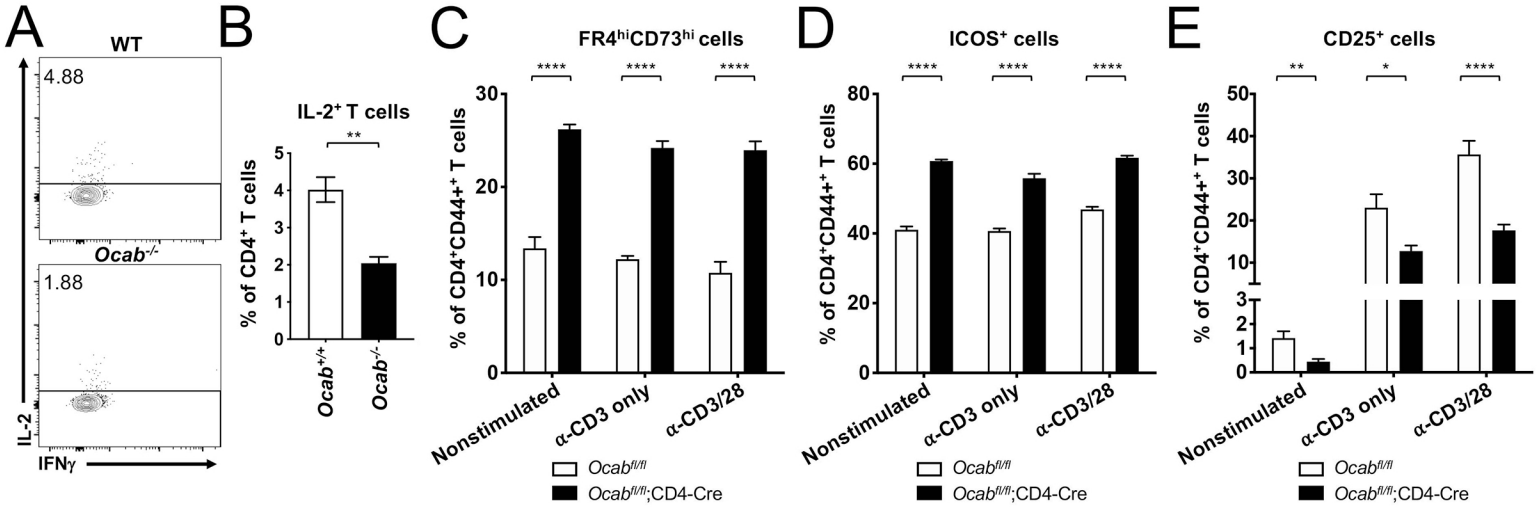

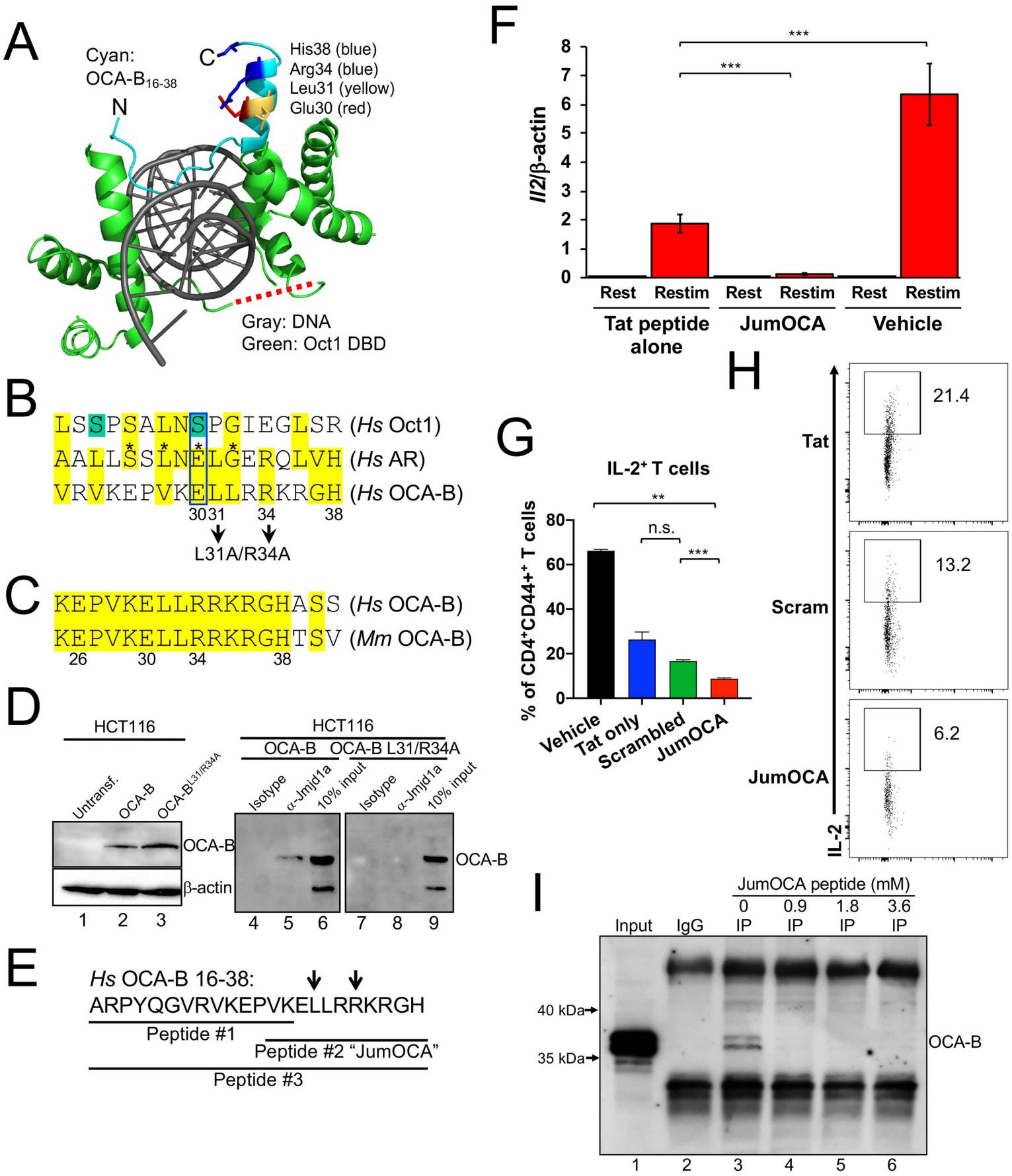
A
Cyan:
OCA-B16-38
C
N
His38 (blue)
Arg34 (blue)
Leu31 (yellow)
Glu30 (red)
Gray: DNA
Green: Oct1 DBD
B
LSSPSALNSPGIEGLSR (Hs Oct1)
AALLSSLNELGERQLVH (Hs AR)
VRVKEPVKELLRRKRGH (Hs OCA-B)
30 31 34 38
L31A/R34A
C
KEPVKELLRRKRGHASS (Hs OCA-B)
KEPVKELLRRKRGHTSV (Mm OCA-B)
26 30 34 38
D
HCT116
Untransf.
OCA-B
OCA-BL31/R34A
OCA-B
β-actin
1 2 3
HCT116
OCA-B
OCA-B L31/R34A
Isotype
α-Jmjd1a
10% input
OCA-B
4 5 6 7 8 9
E
Hs OCA-B 16-38:
ARPYQGVRVKEPVKELLRRKRGH
Peptide #1
Peptide #2 "JumOCA"
Peptide #3
F
Il2/β-actin
Rest
Restim
Tat peptide alone
JumOCA
Vehicle
G
IL-2+ T cells
% of CD4+CD44++ T cells
Vehicle
Tat only
Scrambled
JumOCA
n.s.
H
Tat
Scram
JumOCA
IL-2
21.4
13.2
6.2
I
JumOCA peptide (mM)
0 0.9 1.8 3.6
Input
IgG
IP
40 kDa
35 kDa
OCA-B
1 2 3 4 5 6

Figure 7

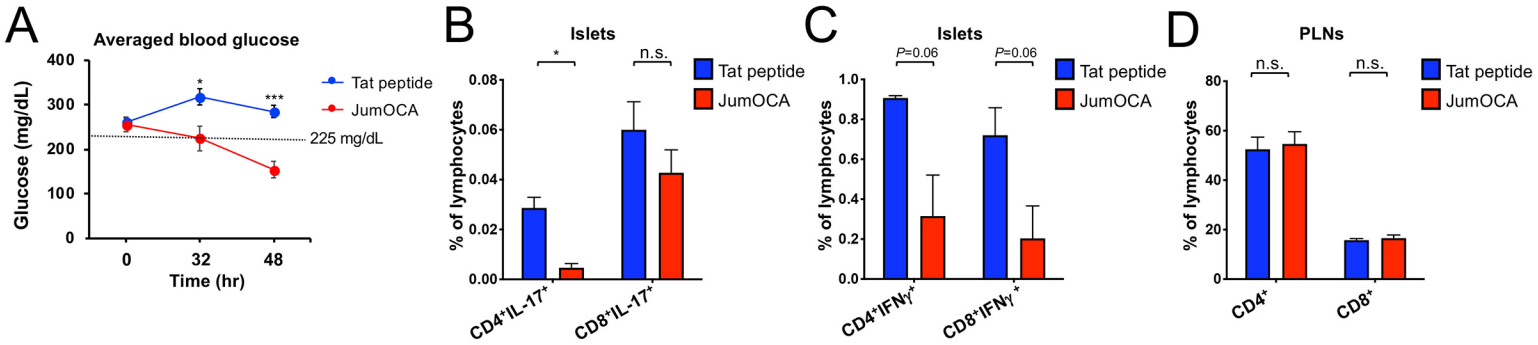
A
Averaged blood glucose
Glucose (mg/dL)
400
300
200
100
0
0
32
48
Time (hr)
*
***
Tat peptide
JumOCA
225 mg/dL
B
Islets
% of lymphocytes
0.08
0.06
0.04
0.02
0.00
*
n.s.
CD4+IL-17+
CD8+IL-17+
Tat peptide
JumOCA
C
Islets
% of lymphocytes
1.0
0.8
0.6
0.4
0.2
0.0
P=0.06
P=0.06
CD4+IFNγ+
CD8+IFNγ+
Tat peptide
JumOCA
D
PLNs
% of lymphocytes
80
60
40
20
0
n.s.
n.s.
CD4+
CD8+
Tat peptide
JumOCA